Phenomenology for the decay of energycontaining eddies in homogeneous MHD turbulence

Murshed Hossain, Perry C. Gray, Duane H. Pontius Jr., William H. Matthaeus, and Sean Oughton

Citation: Physics of Fluids (1994-present) **7**, 2886 (1995); doi: 10.1063/1.868665
View online: http://dx.doi.org/10.1063/1.868665
View Table of Contents: http://scitation.aip.org/content/aip/journal/pof2/7/11?ver=pdfcov
Published by the AIP Publishing

Phenomenology for the decay of energy-containing eddies in homogeneous MHD turbulence

Murshed Hossain,[a] Perry C. Gray, Duane H. Pontius, Jr., and William H. Matthaeus
Bartol Research Institute, University of Delaware, Newark, Delaware 19716

Sean Oughton
Department of Mathematics, University College, London, WC1E 6BT, United Kingdom

(Received 28 April 1995; accepted 25 July 1995)

We evaluate a number of simple, one-point phenomenological models for the decay of energy-containing eddies in magnetohydrodynamic (MHD) and hydrodynamic turbulence. The MHD models include effects of cross helicity and Alfvénic couplings associated with a constant mean magnetic field, based on physical effects well-described in the literature. The analytic structure of three separate MHD models is discussed. The single hydrodynamic model and several MHD models are compared against results from spectral-method simulations. The hydrodynamic model phenomenology has been previously verified against experiments in wind tunnels, and certain experimentally determined parameters in the model are satisfactorily reproduced by the present simulation. This agreement supports the suitability of our numerical calculations for examining MHD turbulence, where practical difficulties make it more difficult to study physical examples. When the triple-decorrelation time and effects of spectral anisotropy are properly taken into account, particular MHD models give decay rates that remain correct to within a factor of 2 for several energy-halving times. A simple model of this type is likely to be useful in a number of applications in space physics, astrophysics, and laboratory plasma physics where the approximate effects of turbulence need to be included. © *1995 American Institute of Physics.*

I. INTRODUCTION

Turbulence theory is far from a completed subject in hydrodynamics and is both more complex and less well understood in magnetohydrodynamics (MHD). Turbulence is studied as a fundamental physical process, but there is also a need to understand how turbulence affects natural and man-made complex systems. Driven by these applications, the subject of turbulence modeling (see, e.g., Ref. 1) has evolved in parallel to mathematical turbulence theory. There have been at least several recent efforts to develop MHD turbulence models.[2–5] At present, MHD turbulence is clearly recognized as being of central importance to numerous subjects of ongoing research, e.g., the sun, the heliosphere, space plasmas, and cosmic ray acceleration and propagation. While these applications may eventually require precise accounts of the dynamical evolution of turbulence, the immediate need is to include reasonable quantitative estimates of MHD turbulence in dynamical models appropriate to the specific application.

In the present paper we describe and evaluate several simple models of MHD turbulence, touching upon hydrodynamic models as well. The models include only a minimum number of energy variables and length scales, and are based upon ideas already found in the literature, and we evaluate their performance relative to a set of accurate spectral method simulations. This permits an assessment of the level of accuracy that might be expected when such models are built into applications in forms that may resemble hydrodynamic K-ϵ models.[1] Our main conclusion is that turbulent decay rates can be reliably estimated to within a factor of two for a duration of at least several energy-halving times.

II. BACKGROUND AND APPROACH

Our principal goal is to discuss and evaluate several phenomenological models for the decay of energy and related quantities in homogeneous incompressible MHD turbulence. Our treatment will extend only to simple "one-point models" that involve no specific information about the wavenumber spectra of excitations. Even within this class of models our treatment will be incomplete, since a large number of models of this type are possible. Most of the physical principles for constructing models of MHD turbulence are familiar in the literature,[6–12] and we will draw freely from these sources.

The incompressible MHD equations involve the solenoidal fluid velocity $\mathbf{u}$ and the magnetic field $\mathbf{B}$. The magnetic field $\mathbf{B}$ is written as the sum of a locally uniform mean value, $\mathbf{B}_0$, and a fluctuating part $\mathbf{b}$. The equations are cast in Alfvén speed units,[13] in which the magnetic field is measured in terms of its associated Alfvén speed ($\mathbf{B}\rightarrow(4\pi\rho)^{-1/2}\mathbf{B}$, uniform mass density ρ), and the characteristic speed is chosen to be that associated with the fluctuations. The dynamical equations are conveniently written using Elsässer variables,[14]

$$\mathbf{z}_{\pm}=\mathbf{u}\pm\mathbf{b}, \tag{1}$$

as

$$\frac{\partial\mathbf{z}_{\pm}}{\partial t}=-\nabla p^{T}-\mathbf{z}_{\mp}\cdot\nabla\mathbf{z}_{\pm}\pm\mathbf{V}_{\mathrm{A}}\cdot\nabla\mathbf{z}_{\pm}+\mathbf{S}_{\pm}\,. \tag{2}$$

[a]Corresponding author: 302-831-8117; fax 302-831-1843; e-mail: hossain@bartol.udel.edu

 1070-6631/95/7(11)/2886/19/$6.00

TABLE I. Simulation parameters for 64^3 spectral simulations: mean magnetic field strength B_0, viscosity ν, resistivity μ, time step dt, halving time for total energy $t(E_0/2)$, time of maximum enstrophy $t(\Omega_{\max})$, initial normalized cross helicity $\sigma_c=2H_c/E=(Z_+^2-Z_-^2)/(Z_+^2+Z_-^2)$, and the initial Alfvén ratio $r_A=E_v/E_b$ (all times given in units of characteristic time τ).

3D MHD Simulation Parameters										
Run number	B_0	ν	μ	dt	$t(E_0/2)$	$t(\Omega_{\max})$	σ_c	r_A	Initial k-range	Knee
07	0	1/200	1/200	1/400	0.67	0.3	0	1	1–15	4
08	1	1/200	1/200	1/400	0.75	0.3	0	1	1–15	4
09	0	1/200	1/200	1/400	2.5	1.6	0	1	1–3	4
10	0.1	1/200	1/200	1/400	2.55	1.6	0	1	1–3	4
11	1	1/200	1/200	1/400	3.02	1.8	0	1	1–3	4
12	3	1/200	1/200	1/1250	4.45	2.2	0	1	1–3	4
15	0	1/200	1/200	1/400	0.77	0.0	0.43	3	3–15	2
16	0	1/200	1/200	1/400	0.81	0.3	0.43	1	3–15	2
17	0	1/200	1/200	1/400	0.85	0.4	0.43	1/3	3–15	2
18	0	1/200	1/200	1/400	0.68	0.0	0	3	3–15	2
19	0	1/200	1/200	1/400	0.77	0.4	0	1/3	3–15	2
20	8	1/200	1/200	1/3200	4.67	2.4	0	1	1–3	4
22	0	1/200	NS	1/400	0.81	0.3	NS	NS	1–15	4
23	3	1/200	1/200	1/1250	1.25	0.0	0.55	1	1–15	4
24	0	1/200	1/200	1/400	1.1	0.0	0.8	1	1–15	4
25	0	1/300	NS	1/400	0.75	0.2	NS	NS	1–25	4
26	8	1/200	1/200	1/3200	1.4	0.0	0.55	1	1–15	4
27	1	1/250	1/250	1/400	1.54	0.8	0	1	1–8	3
28	1	1/200	1/200	1/400	0.95	0.3	0.55	1	1–15	4
29	0	1/200	1/200	1/400	0.84	0.3	0.55	1	1–15	4

Dissipation due to a small viscosity ν and resistivity μ, which act mainly at the small scales, are represented by $\mathbf{S}_\pm$. Note that in this system of units the Alfvén speed associated with the mean magnetic field is $\mathbf{V}_A=\mathbf{B}_0$.

For homogeneous MHD turbulence we are particularly interested in the dynamical behavior of the fluctuation energy per unit mass, $E=\langle|\mathbf{u}|^2+|\mathbf{b}|^2\rangle/2=\langle|\mathbf{z}_+|^2+|\mathbf{z}_-|^2\rangle/4$, and the fluctuation cross helicity density, $H_c=\langle\mathbf{u}\cdot\mathbf{b}\rangle$. These quantities are rugged invariants of the ideal MHD equations and particularly relevant to the theory of turbulent spectral transfer.[15–18] The so-called Elsässer energies $Z_+^2=\langle|\mathbf{z}_+|^2\rangle$ and $Z_-^2=\langle|\mathbf{z}_-|^2\rangle$ are equivalent ideal invariants. However, no combination of these invariants distinguish whether energy resides in the magnetic or velocity field. That property is measured by the 'residual energy' or 'energy difference' $D=\langle|\mathbf{u}|^2-|\mathbf{b}|^2\rangle=\langle\mathbf{z}_+\cdot\mathbf{z}_-\rangle$, which, unlike the energy and cross helicity, is not an ideally conserved quantity. This fact makes a significant difference to the development of phenomenological models. The amount of E or H_c present is not modified by the nonlinear terms that mediate spectral transfer from the large energetic eddies through the inertial range (if one is present). In the idealized high Reynolds number limit, these quantities can change only when excitations reach the dissipative scales. In contrast, the dynamical couplings can change the value of the energy difference D. In particular, both nonlinear and wave-like couplings can repartition kinetic and magnetic fluctuation energies.

In the following section we will review and evaluate a familiar one-point energy decay model for homogeneous hydrodynamic turbulence. This will involve one energy and a single length scale. In contrast MHD phenomenology has a greater complexity. To treat cross helicity effects, the theory needs to include both Z_+^2 and Z_-^2, as well as at least one length scale. A second length scale can easily be included, as can dependence upon D, at least in principle.

To provide a data base for comparison with the models, we assembled a set of three-dimensional MHD numerical simulations, employing a Fourier spectral (Galerkin)[19,20] method in periodic geometry. The runs that enter into the discussion in this paper use a code with spatial resolution 64^3, a full dealiasing algorithm, and viscosity equal to resistivity, usually with dimensionless value 1/200. Dealiasing is achieved by extending arrays to 3/2 their original sizes by padding zeroes. The properties of the various runs are recorded in Table I for reference in the later discussion. We have also tabulated, for each run, the energy halving times, $t(E_0/2)$, and the time $t(\Omega_{max})$, when the enstrophy is the maximum. As we can see, the energy halving times range from 0.67 to 4.67: varying by almost an order of magnitude. For the runs with initial broad spectrum the enstrophy maximum occurs at or near $t=0$. The time at which j^2 is maximum in its evolution is within 10% of $t(\Omega_{max})$.

To illustrate the variety of behavior seen in these simulations, we refer first to Fig. 1, showing the time history of E for five simulations, designated as Runs 07, 15, 18, 20, and 25. Four of the runs exhibit somewhat similar energy decay and are grouped together. Run 18, which decays most quickly, has nearly zero cross helicity H_c and non-zero energy difference D. Run 20, which decays most slowly, is the only one of these five runs with a large-scale mean magnetic field; here $B_0=8$. Run 25 is a purely Navier–Stokes (NS) hydrodynamic run. The other two runs are distinguished by values of H_c and D which are both non-zero (Run 15) and both ≈ 0 (Run 07). The four panels of Fig. 2 illustrate the behavior of the Elsässer energies $Z_\pm^2$ for Runs 7, 15, 18, and 20. Runs 15 and 20 (panels 2b and 2d) show that initially

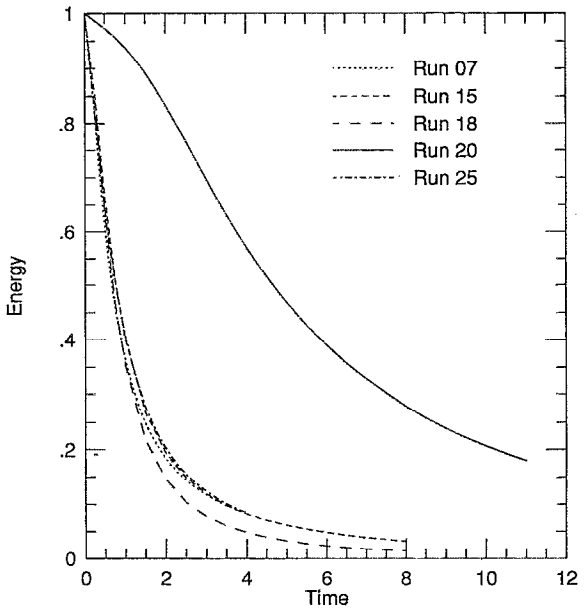

FIG. 1. Time history of total energy for five different runs showing a wide range of decay rates.

unbalanced Z_+^2 and Z_-^2 remain so, causing the phenomenon of dynamic alignment,[21–23,11,8] in which the value of normalized cross helicity $\sigma_c = 2H_c/E = (Z_+^2 - Z_-^2)/(Z_+^2 + Z_-^2)$ grows in time. The magnetofluid become progressively more "Alfvénic" as the turbulence is increasingly dominated by fluctuations of one sense. In Runs 7 and 18 (panels 2a and 2c) there is only a small difference between the two Elsässer fields, although there is a slight growth in Run 07.

Figure 3 shows the progression of the wavenumber spectrum in time for Run 07, which, in a sense to be defined below (section VII B), is most like Navier–Stokes flow, even though magnetic and kinetic energies are nearly equal. The spatial resolution and Reynolds numbers of our simulations ($\nu^{-1} \approx 200$) are necessarily lower than would be optimal for exploring high Reynolds number turbulent decay. Nevertheless, the spectra indicate a reasonably good resolution of dynamically important spatial scales, a hint of a near-power law inertial range (over less than a decade in wavenumber), and a rollover at an energy-containing scale near dimensionless wavenumber 5 or thereabouts (Fig. 3).

These simulations illustrate the phenomena that we seek to describe with approximate models for the decay of global energy variables in MHD. The MHD results have a greater variety of behavior than the Navier–Stokes result (Run 25), which has $Z_+^2 = Z_-^2 = D$. Therefore, before describing and evaluating the MHD phenomenology, we review and analyze the simpler and better known phenomenology for the decay of energy-containing eddies in hydrodynamics.

III. DECAY OF ENERGY-CONTAINING EDDIES IN HYDRODYNAMIC TURBULENCE

A simple and reasonably accurate phenomenological model exists for turbulent hydrodynamic energy decay at high Reynolds number, such as that plotted in Fig. 1 for Run 25. This model has a rich history that provides important background and motivation for development of MHD turbulence models. Historically, Taylor,[24] Karman and Howarth,[25] and others investigated the decay of (twice) the total energy per unit mass, u^2, in homogeneous isotropic turbulence. Taylor's theory obtained a t^{-2} time dependence when the correlation (outer) scale ℓ was assumed constant. Karman proposed a *self preservation hypothesis* that the correlation functions preserve their shape according to a similarity law during the decay.

For homogeneous turbulence, the self preservation hypothesis was supposed to apply to all spatial scales that are large compared to the viscous or dissipation scale η. As described by Batchelor,[26] various experimental observations, particularly in wind tunnels,[27,28] suggest that approximately $u^2 \propto t^{-1}$, with the length scale $\ell \propto \sqrt{t}$. Such dynamic evolution is fully consistent with the self-preservation assumption. Since most of the fluctuation energy is found at scales $\lambda \gg \eta$, this behavior is identified as the decay law for the total energy, i.e., the decay law for the energy-containing eddies. The only scales not included are those near the dissipation scale or smaller, and structures at such large scales that the homogeneity assumption breaks down.

The approach of Karman and Howarth,[25] Kolmogoroff,[29–31] Batchelor,[26] and others motivates a family of decay laws by associating the decay time or spectral transfer time, τ_s, with the characteristic nonlinear time, $\tau_{nl} = \lambda/u$, obtained by dimensional analysis alone. Here, λ is a length-scale characterizing the energy-containing eddies. Usually it will be the correlation scale or integral scale.[26] The nonlinear time also equals the characteristic eddy lifetime and is assumed to be the only time scale relevant to the problem. One can immediately write an energy equation

$$\frac{du^2}{dt} = -\alpha \frac{u^2}{\tau_{nl}} = -\alpha \frac{u^3}{\lambda}. \tag{3}$$

Similarly by dimensional analysis a λ equation is written to supplement (3):

$$\frac{d\lambda}{dt} = \beta \frac{\lambda}{\tau_{nl}} = \beta u. \tag{4}$$

Here, α and β are positive constants of order unity that are formally undetermined by dimensional analysis.

Equations (3)–(4) define a complete phenomenological model for the evolution of the energy-containing eddies. The system of equations can be solved readily upon observing that $u^2 \lambda^{\alpha/\beta} =$ const, which yields

$$u(t) = u(t_0)[1 + A(t - t_0)]^{-\alpha/(\alpha+2\beta)}, \tag{5}$$

$$\lambda(t) = \lambda(t_0)[1 + A(t - t_0)]^{2\beta/(\alpha+2\beta)}. \tag{6}$$

The characteristic time for development of self-similar decay is $A = u_0(\alpha + 2\beta)/(2\lambda_0)$, where the zero subscript signifies evaluation at t_0. At large times $\lambda/u \propto t$ becomes independent of the parameters α and β.

For the choice of constants $\alpha = 1$ and $\beta = 1/2$ in (3) and (4), the solutions (5)–(6) behave at large time as

$$u^2 \approx (t - t_0)^{-1}, \tag{7}$$

$$\lambda \approx (t - t_0)^{1/2}, \tag{8}$$

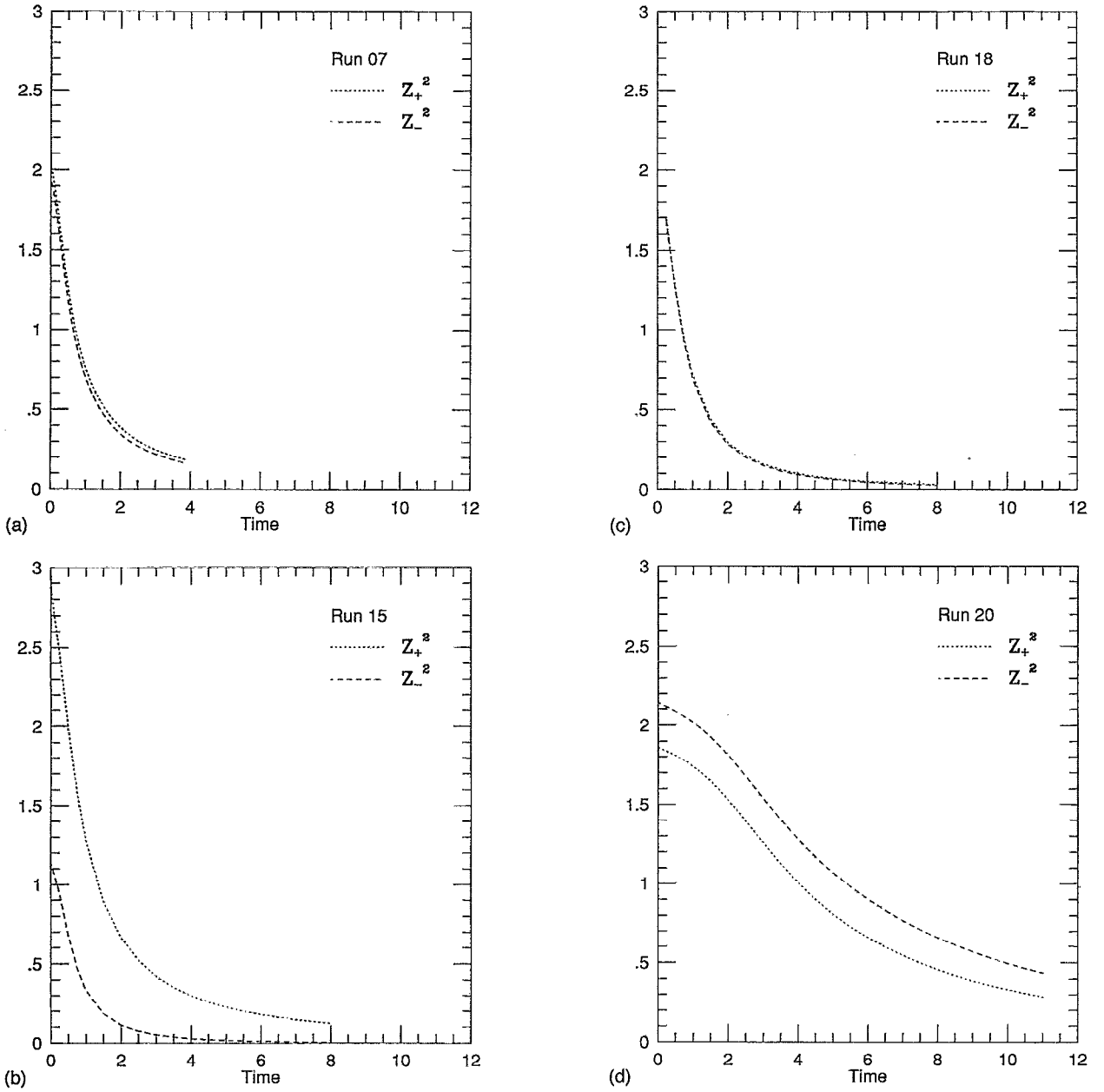

FIG. 2. Time history of $Z_{\pm}^2$ for four typical runs. (a) Run 07: pseudo NS, (b) Run 15: non-zero cross helicity and D, (c) Run 18: zero cross helicity but $D=0$, and (d) Run 20: Large mean field, zero cross helicity, zero D.

which is precisely the behavior associated with self-preservation of the shape of the correlation function (in fact, any $\alpha=2\beta$ gives the same result). The simple pair of coupled differential equations $du^2/dt=-u^3/\ell$ and $d\ell/dt=u/2$ that predict this decay law are described, though not emphasized as such, in the same paper by Karman and Howarth.[25] Note that ℓ is a large-scale characteristic dynamical length scale in the Karman and Howarth theory and can depend upon the various length scales that enter into the description of the large-scale turbulence. Here, it is associated simply with the correlation scale λ. Various corrections to the t^{-1} law[30,32,33] emerge by departing from either strict homogeneity or strict dynamical self-preservation at the very largest scales. These refinements improve the theoretical underpinnings as well as agreement with experiments, but they do not significantly alter the exponents for energy decay and growth of the correlation scale.

In contrast to these theories, assuming a stronger condition of similarity, that is, scale-free self-preservation (or self-similarity), leads to inertial range theory.[29] This additional property implies a power-law dependence of the energy spectrum across a subrange of wavenumbers and is appropriate only for fluctuations with characteristic lengths, λ', satisfying $\ell \gg \lambda' \gg \eta$. Thus, the range of wavenumbers associated with the inertial range is a subset of those to which the energy-decay theories of Taylor and Karman may apply.

Kolmogoroff's version of the energy-decay theory[34] was perhaps the first to write clearly a pair of coupled differential

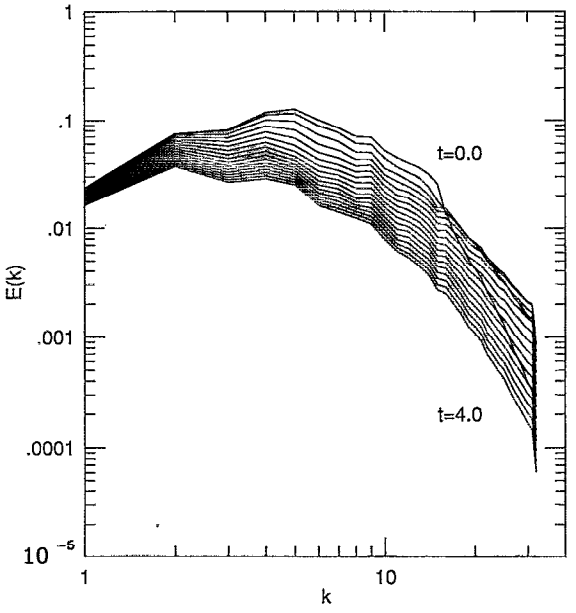

FIG. 3. Snap shots of omni-directional energy spectra for MHD Run 07 (pseudo Navier–Stokes run) for different times from $t=0$ to $t=4$.

equations that determined the approximate decay of energy. Kolmogoroff used a b-ω model, representing $b \sim u^2/3$ and $\omega \sim \ell/u$. The version of Kolmogoroff's two-equation model discussed by Spalding[34] includes inhomogeneous effects as well and can be considered the antecedent of both hydrodynamic and MHD turbulence modeling. Both Kolmogoroff's[30,34] and Saffman's[33] models can be obtained by appropriate choices of the parameters α and β in Eqs. (3) and (4).

A. Numerical demonstration

For our numerical comparisons we use data from three-dimensional simulations of incompressible fluid (and magnetofluid) turbulence based on a Fourier spectral method[19,20] in a periodic box of size $(2\pi)^3$. Details of the initial conditions are given in Appendix A, and a summary of the simulations discussed here appears as Table I. Run 25 in the table is relevant to the hydrodynamics case.

To apply the phenomenological model (3)–(4), we must first calculate the length scale λ for the energy-containing eddies. Our definition is based upon the longitudinal integral scale used in isotropic turbulence theory,[26]

$$\lambda = \frac{\pi \int dk \hat{E}(k)/k}{\int dk \hat{E}(k)}, \tag{9}$$

where $\hat{E}(k)$ is the omni-directional energy spectrum, and the denominator is equal to the total energy per unit mass E. For the discrete wave-vector space of the simulation it is more convenient to use the modal energy spectrum $E(\mathbf{k})$, so that

$$\lambda = \frac{\pi}{E} \sum_{\mathbf{k}} \frac{E(\mathbf{k})}{|\mathbf{k}|}. \tag{10}$$

The total energy is $E = \Sigma_{\mathbf{k}} E(\mathbf{k})$. In our simulations, the evolution of λ is limited by the fact that there is a largest allowed wavelength, i.e., the scale of the spatial periodicity. The phenomenology has been developed for turbulence in an infinite domain, so we introduce a finite box size correction to the behavior of λ:

$$\frac{d\lambda}{dt} = \beta u \left[1 - \frac{\lambda}{\lambda_{\max}} \right], \tag{11}$$

where $\lambda_{\max}$ is a scale associated with the box size. We have usually taken $\lambda_{\max} = \pi/2$.

To assess the accuracy of the model represented by (3) and (11), we accumulate simulation data and subject it to several tests, the results of which are illustrated in Fig. 4. First, the numerical value of the decay rate $(du^2/dt)_{\text{sim}}$ is calculated at regular intervals, using finite differences. An effective α at each time is obtained by dividing the magnitude of $(du^2/dt)_{\text{sim}}$ by the value of u^3/λ computed using the simulation data for the same instant. Panel 4a plots the putative values of α obtained in this way. Clearly, α is not strictly constant as assumed in the model. Part of this is caused by a start-up transient in the dynamics, and we do not expect Eq. (3) to apply during the first characteristic time (about 1 time unit on the abscissa). In contrast, during the remainder of the simulation, α remains fairly steady, and the model estimates the instantaneous decay rate of total energy to within a factor of 1.5 to 2. A similar test of Eq. (11) is shown in Fig. 4b, where the numerically determined time rate of change of λ is compared with the right hand side of (11) to extract an effective β at each time. The values of β are of order unity, and between $t=2$ and 3 there is a plateau near $\beta \approx 0.5$. During this same period, we see from Panel 4a that $\alpha \approx 0.9$.

Figures 4a and 4b indicate that the simple family of Navier–Stokes phenomenologies (3) and (11) work reasonably well in predicting the instantaneous decay rate, using phenomenological constants $\alpha \approx 0.9$ to 0.95 and $\beta \approx 0.4$ to 0.5 that are not far from the values associated with the self-preservation hypothesis. A more difficult challenge for the model is to explain the time history of the decaying energy, since in this case the errors in estimating the decay rate are cumulative. Figure 4c shows a comparison of $E(t)$ for Run 25 with the integrated solution of Eqs. (5) and (11), starting with initial data from simulation time $t=1$ to avoid start-up transients. The constants used in the comparison were $\alpha=0.95$ and $\beta=0.45$. Similarly, the results for the time history of λ are shown in Fig. 4d, again comparing the simulation results in Run 25 with the solution of (11), integrating once again from $t=1$ to 4. The theory and simulations are in reasonable agreement, particularly when we recall the relatively low Reynolds number of the simulation.

Evidently, the simple phenomenological model can describe homogeneous hydrodynamic turbulence in a finite box satisfactorily, once the finite size effect is taken into account. Finite box size is a severe limitation on the growth of λ. In the above comparisons, the length scale λ does not change significantly over the entire period of evolution. As a result, the comparison may test mainly the structure of the energy

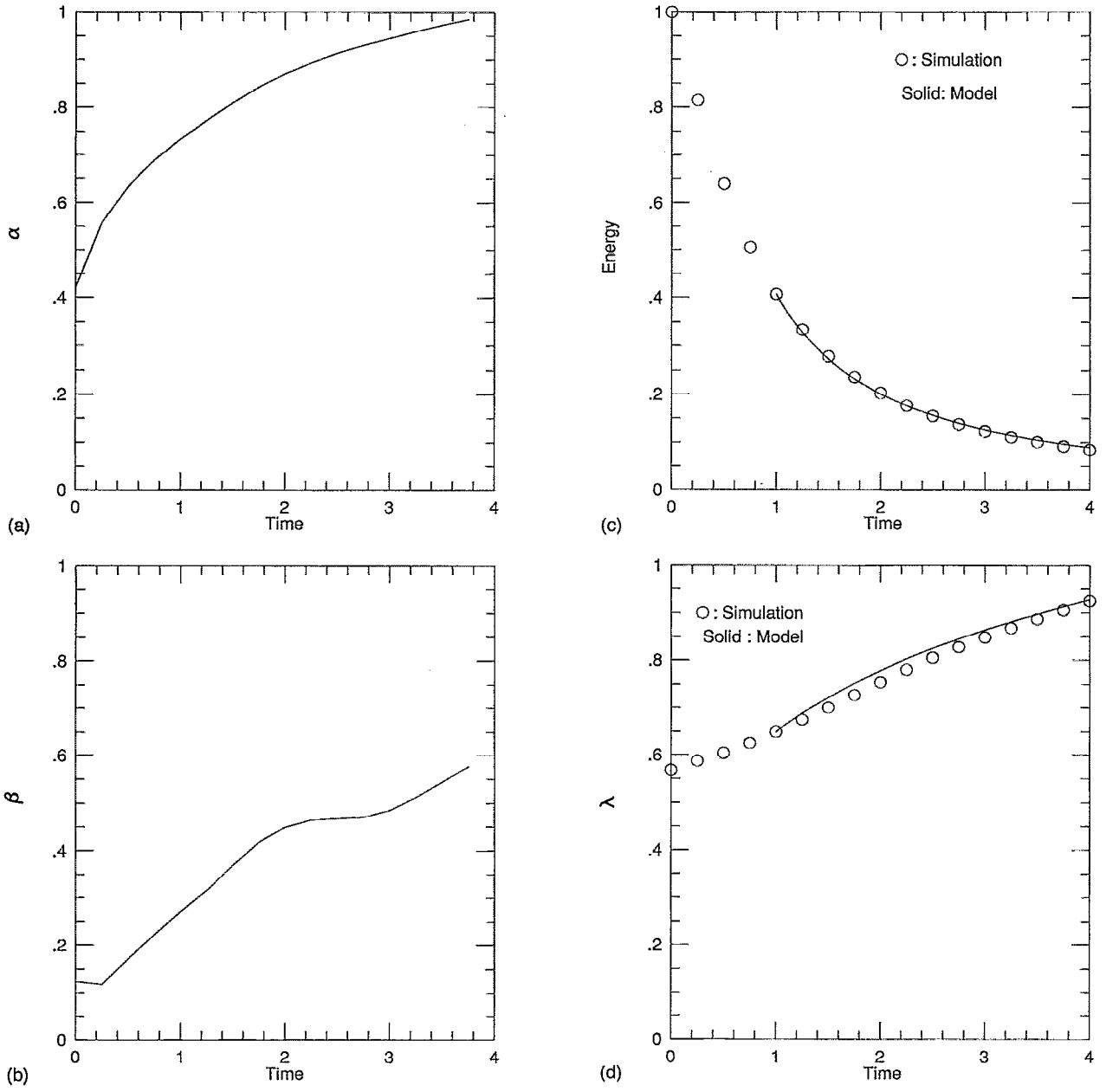

FIG. 4. Computed (a) α and (b) β using the data from the simulation [cf. Eqs. (3) and (11)] for the NS Run 25 at various times. Evolution of (c) energy and (d) λ obtained by integrating model equations (3) and (11) using a pair of best fit α and β starting at $t=1$. Superimposed discrete points are data from the simulation.

decay equation. As in the comparison of instantaneous decay rates, we see that order unity constants work well.

Note that if λ is strictly held constant then $\beta=0$ identically. Then Eq. (5) implies $u\sim t^{-1}$. A recent experiment[35] with length scale of the energy containing eddies approximately constant did find $u\sim t^{-1}$ consistent with Taylor's theory.[24]

IV. PHENOMENOLOGICAL MODELS OF MHD DECAY

We now consider several one-point models for decaying MHD turbulence. They involve the evolution of the mean-square Elsässer variables $Z_{\pm}^2=\langle|\mathbf{z}_{\pm}|^2\rangle$. The complete model will also include an evolution equation for the length scales $\lambda_{\pm}$ associated with $Z_{\pm}^2$, or possibly a single length scale that is a composite of these two. The length scales $\lambda_{\pm}$, are defined as

$$\lambda_{\pm}=\frac{\pi}{Z_{\pm}^2}\sum_{\mathbf{k}}\frac{|\mathbf{z}_{\pm}(\mathbf{k})|^2}{|\mathbf{k}|}, \tag{12}$$

where $Z_{\pm}^2=\Sigma_{\mathbf{k}}|\mathbf{z}_{\pm}(\mathbf{k})|^2$. For models with just one spatial scale, it is convenient to introduce a weighted combination of the separate $\pm$ scales, of the form $\lambda=(Z_+^2\lambda_++Z_-^2\lambda_-)/(Z_+^2+Z_-^2)$ as suggested by Matthaeus *et al.*[36] Note that when $\lambda_+=\lambda_-$, we use the notation $\lambda\equiv\lambda_{\pm}$.

Another quantity that can enter the models is the mean correlation of the two Elsässer fields $D=\langle \mathbf{z}_+ \cdot \mathbf{z}_- \rangle$, which is also proportional to the difference between the kinetic and magnetic energies, $\langle \mathbf{u}^2 - \mathbf{b}^2 \rangle$. We have investigated several versions of the models in which the decay of $Z_\pm^2$ depends upon D. However, because D generally decays very rapidly to values near zero, it has little influence on the model comparisons. Therefore, to keep the models simple, we only present results from models in which D does not influence the decay of $Z_\pm^2$. We will briefly discuss a model equation for the decay of D itself in a later section.

Kraichnan[6] and Dobrowolny *et al.*[21,22] applied the approach of Karman and Kolmogoroff for hydrodynamic models to the turbulent decay of the Elsässer energies $Z_\pm^2$ in MHD. For the present purposes, the first step is to write the decay of $Z_\pm^2$ in terms of spectral transfer times $\tau_s^\pm$,

$$\frac{dZ_+^2}{dt} = -\frac{Z_+^2}{\tau_s^\pm}. \tag{13}$$

This equation defines $\tau_s^\pm$, but by considering the structure of the dynamical equations (2), these spectral transfer times can be estimated in terms of several characteristic time scales. The first is $\tau_{nl}^\pm$, the characteristic nonlinear time, generalized for MHD in Elsässer representation,[21]

$$\tau_{nl}^\pm = \frac{\lambda_\pm}{Z_\mp}. \tag{14}$$

This time scale represents the approximate rate at which an energy-containing eddy decays due to the nonlinear term in (2), which arises from correlations with turbulent structures of the other sense. Consequently, the typical lifetime of these triple correlations, $\tau_3^\pm$, is also important. In addition, energy decay has been argued to depend upon wave-propagation effects that are present, represented by a characteristic Alfvénic time scale $\tau_A^\pm$. The superscript $\pm$ on each of these variables admits the possibility that they are generally different for the two Elsässer fields. Each of these quantities has been discussed previously,[6,7,10–12] but mainly in the context of inertial range phenomenology, and then in essentially an isotropic turbulence approximation. Therefore, one reason for investigating several phenomenological models for MHD energy decay is that it is unclear how these earlier inertial range arguments are properly applied in the energy-containing range. Taking into account possible ambiguities concerning the definitions of the time scales themselves, we expect that the spectral transfer times will depend on the various characteristic scales so that $\tau_s^\pm = \tau_s^\pm(\tau_{nl}^+, \tau_{nl}^-, \tau_A^+, \tau_A^-, \tau_3^+, \tau_3^-)$.

A. Model A

In connection with the inertial range Kraichnan[6] argued that the steady energy-transfer rate of $\pm$ fields must be directly proportional to the lifetime of the triple correlations τ_3. He then pointed out that the triple lifetime should be comparable to the period of the relevant Alfvén waves due to the mean magnetic field, when propagation is sufficiently strong that $\tau_A \ll \tau_{nl}$. The suggestion has been made that the inertial range triple correlation also decays due to propagation effects associated with the fluctuating magnetic field.[7] Under the isotropy assumption, the wave period at wavenumber k is of order $(kV_A)^{-1}$ (the Alfvén speed in our units is $V_A = B_0$). These ideas can be directly carried over to the energy-containing range by using $\lambda_\pm$ in place of k^{-1}. This leads to a characteristic Alfvén time

$$\tau_A^\pm = \frac{\lambda_\pm}{\sqrt{V_A^2 + b^2}}. \tag{15}$$

The triple correlation also decays due to the nonlinear process characterized by τ_{nl}, but the Kraichnan phenomenology[6] neglects this effect, because of the assumed strength of the mean magnetic field. For cases where both effects are important, one possible way to write the total rate of triple decorrelation is as a sum of the hydrodynamic and the mean field rates[12]:

$$\frac{1}{\tau_3^\pm} = \frac{1}{\tau_{nl}^\pm} + \frac{1}{\tau_A^\pm}. \tag{16}$$

We can combine the triple decorrelation time scales and the hydrodynamic nonlinear times scales to form the spectral time scale[12]:

$$\tau_s^\pm = \frac{(\tau_{nl}^\pm)^2}{\tau_3^\pm}. \tag{17}$$

Estimates of this type for the spectral transfer time in the inertial range, parametrized by wavenumber and dependent upon the cross helicity, have been used by Dobrowolny *et al.*[22] and by Grappin *et al.*[10,11] What we shall refer to as "Model A" consists of using (17) to estimate the spectral transfer time in (13).

The evolution of the length scales $\lambda_\pm$ are given by:

$$\frac{d\lambda_\pm}{dt} = \beta_\pm (\lambda_\pm \epsilon_\pm)^{1/3} \left[1 - \frac{\lambda_\pm}{\lambda_{\max}} \right]. \tag{18}$$

Here, $\epsilon_\pm = Z_\pm^2/\tau_s^\pm$. The last term is the finite box size correction, with $\lambda_{\max} = \pi/2$ assumed here. Model A is a plausible and straightforward extrapolation of existing inertial range phenomenological theory to the global decay problem. It will be compared to numerical simulations in section V. For strong mean magnetic field, Model A is essentially an extension of Kraichnan's model[6] for inertial range spectral transfer into the energy-containing range. When $Z_\pm \ll B_0$, the energy decay equation becomes

$$\frac{dZ_\pm^2}{dt} = -\alpha_\pm \frac{Z_+^2 Z_-^2}{\lambda_\pm B_0}. \tag{19}$$

In a symmetric model for which $\alpha_+ = \alpha_-$ and $\lambda_+ = \lambda_-$, the decay rates of Z_+^2 and Z_-^2 are equal, so their difference remains constant. This difference is proportional to the cross helicity. Therefore, while the total energy decreases, the normalized cross helicity $\sigma_c = 2H_c/E = (Z_+^2 - Z_-^2)/(Z_+^2 + Z_-^2)$ increases. This is the argument originally given by Dobrowolny *et al.*[22] for dynamic alignment in the limit that the triple decay rate is controlled by the Alfvén time.

B. Model B1

There are several ways in which models distinct from Model A but equally plausible can be constructed. One way is to adopt a symmetrized pair of equations for the evolution of the length scales, for example,

$$\frac{d\lambda_\pm}{dt}=\beta_\pm\sqrt{Z_+Z_-}\left[1-\frac{\lambda_\pm}{\lambda_{\max}}\right]. \tag{20}$$

This choice permits a convenient special case to be considered, in which λ_+ and λ_- are assumed to have the same initial value. Because their equations of motion are the same, this allows us to define a single scale $\lambda\equiv\lambda_+=\lambda_+$.

As a separate assumption, the spectral transfer time for Model B is taken to be simply the nonlinear time, i.e., $\tau_s=\tau_{nl}$ (weak B_0). Thus the model dynamical equations are

$$\frac{dZ_+^2}{dt}=-\alpha_+\frac{Z_+^2Z_-}{\lambda}, \tag{21}$$

and

$$\frac{dZ_-^2}{dt}=-\alpha_-\frac{Z_-^2Z_+}{\lambda}. \tag{22}$$

Equations (20), (21), and (22) define Model B1 (with finite box-size correction). Numerical tests of Model B1 are given in the next section. A variant of Model B1 may also be implemented with the $\lambda_\pm$ retaining their separate identities (see Model B2 below).

To examine some analytical consequences of Model B1, for the moment we remove the finite box size correction by formally letting $\lambda_{\max}\to\infty$. The length scale equation becomes

$$\frac{d\lambda}{dt}=\beta\sqrt{Z_+Z_-}. \tag{23}$$

In this form the model affords simple analytical solutions. The system of equations (21), (22), and (23) possesses a conservation property:

$$\frac{d}{dt}(\alpha_-Z_+-\alpha_+Z_-)=0, \tag{24}$$

i.e., $(\alpha_-Z_+-\alpha_+Z_-)=(\alpha_-Z_+^0-\alpha_+Z_-^0)$, where the superscript 0 designates the initial value of the field. Thus, we can eliminate one of the $Z_\pm$'s. Let us define a new variable, Z, such that

$$Z=\alpha_-Z_+-a=\alpha_+Z_-+a, \tag{25}$$

where $a=(\alpha_-Z_+^0-\alpha_+Z_-^0)/2$.

Now we have two simultaneous equations to solve:

$$\frac{dZ}{dt}=-\frac{Z^2-a^2}{2\lambda}, \tag{26}$$

$$\frac{d\lambda}{dt}=\frac{\beta}{\sqrt{\alpha_+\alpha_-}}\sqrt{Z^2-a^2}. \tag{27}$$

These two equations can be solved by dividing (26) by (27) and using the conservation property (24). Details of the general solution are relegated to Appendix B. Here, we discuss the special case when $Z_+^0=Z_-^0$, i.e., $a=0$. Thus, $Z_+=Z_-=Z$. Then, the solution to Model B1 becomes,

$$Z(t)=Z^0[1+A(t-t_0)]^{-\bar\alpha/(\bar\alpha+2\beta)} \tag{28}$$

where $\bar\alpha\equiv\sqrt{\alpha_+\alpha_-}$ and

$$A=\frac{Z^0(1+2\beta/\bar\alpha)}{2\lambda^0}. \tag{29}$$

For the case of $\alpha_+=\alpha_-$ this solution reduces to the Navier–Stokes case described in section III. We return to this question of the Navier–Stokes limit of MHD in section VII B.

C. Model B2

As a third possibility, we form a model closely related to Model B1 but with different dynamical equations for the length scales. We group this along with Model B1 under the label "Model B" but designate it specifically as Model B2. It is formed by writing $d\lambda_\pm/dt\sim\lambda_\pm/\tau_{nl}^\pm$, or, using Eq. (14),

$$\frac{d\lambda_\pm}{dt}=\beta_\pm Z_\mp. \tag{30}$$

No correction for finite box size is included explicitly in (30), although in the comparisons with simulations we incorporate a factor $[1-\lambda_\pm/\lambda_{\max}]$ as was done in Eq. (20). Note that when one of the fields $Z_\pm$ vanishes, the length scale of the nonvanishing field ceases to evolve. This is consistent with the fact that the spectral transfer ceases when one of the fields is zero. The length scale of the vanishing field formally grows according to (30), but this does not violate any principle because no excitation is present.

Model B2 makes use of the nonlinear times in Eq. (30), with distinct length scales, so that the appropriate dynamical equations for the energy decay are [see (13)]

$$\frac{dZ_+^2}{dt}=-\alpha_+\frac{Z_+^2Z_-}{\lambda_+}, \tag{31}$$

and

$$\frac{dZ_-^2}{dt}=-\alpha_-\frac{Z_-^2Z_+}{\lambda_-}. \tag{32}$$

In section V, Model B2 will be evaluated using the simulation data base, along with Models A and B1.

Model B2 possesses a class of conservation laws. For arbitrary $q_\pm\neq1$, we find that

$$\frac{d}{dt}[\lambda_\pm Z_\pm^{q_\pm}]=0, \tag{33}$$

where the exponents $q_\pm$ satisfy

$$q_\pm=\frac{2\beta_\pm}{\alpha_\pm}, \tag{34}$$

and we designate the constant values $C_\pm=\lambda_\pm Z_\pm^{q_\pm}$. These conservation laws permit us to easily obtain analytic solutions. They can be cast into a more revealing constraint between Z_+ and Z_-:

$$\frac{Z_+^{1-q_+}(t)-Z_+^{1-q_+}(t_0)}{Z_-^{1-q_-}(t)-Z_-^{1-q_-}(t_0)}=\frac{(\alpha_+C_-)(1-q_+)}{(\alpha_-C_+)(1-q_-)}, \tag{35}$$

which is constant. This allows the solution to be reduced to an integral for $Z_\pm$. Nice solutions are found for integer values of q_+ and q_-.

For $q_\pm=1$, the special case where $2\beta_\pm=\alpha_\pm$, the above conservation laws take the form:

$$\frac{d}{dt}[\lambda_\pm Z_\pm]=0, \tag{36}$$

which can be integrated to give

$$\frac{Z_+(t)}{Z_+(t_0)}=\left[\frac{Z_-(t)}{Z_-(t_0)}\right]^C, \tag{37}$$

where $C=\alpha_+C_-/(\alpha_-C_+)$. This connection between Z_+ and Z_- can be used to eliminate one of the $Z_\pm$ yielding the closed form solutions,

$$Z_+(t)=Z_+(t_0)\left[1+\frac{(C'+1)\alpha_+Z_-(t_0)(t-t_0)}{2C_+Z_+^{2C'+1}(t_0)}\right]^{-1/(C'+1)}, \tag{38}$$

and

$$Z_-(t)=Z_-(t_0)\left[1+\frac{(C'+1)\alpha_+Z_-(t_0)(t-t_0)}{2C_+Z_+^{2C'+1}(t_0)}\right]^{-C'/(C'+1)}, \tag{39}$$

where $C'=1/C$.

The conservation laws (36) bear a strong resemblance to the Navier–Stokes case (3) and (4) which, when $2\beta=\alpha$, admits the conservation property

$$\frac{d}{dt}[\lambda u]=0. \tag{40}$$

If the Z_+ and Z_- are equal then the MHD Model B2 reduces to two independent models (one for the + variables, one for the − ones), each like the Navier–Stokes model. Moreover, if there is only one length scale $\lambda=\lambda_+=\lambda_-$ then Models B1 and B2 are identical to one another.

V. NUMERICAL EVALUATION OF THE MODELS

A. Model A

To evaluate the accuracy of Model A we begin by testing whether Eq. (13) represents a reasonable estimate of the instantaneous decay rates of $Z_\pm^2$ obtained from the numerical simulations. For the decay of Z_+^2, Model A uses (14)–(17) to compute the right hand side of (13). This value is compared to the value of dZ_+^2/dt determined directly from the simulations by taking finite differences. The ratio of the model value for dZ_+^2/dt to the value determined from the simulation can be thought of as a time-dependent value of α_+, which is supposed constant in the model. Figure 5 depicts the time-dependent values of α_+ from the eighteen MHD simulations in Table I. One sees immediately that the general trend in time is for α_+ to increase. For a few runs this increase is by more than a factor of ten, and for some parameters the increase is by a factor of 25 by $t=8$. In this and other similar figures we do not label individual runs since we are interested to study the general behavior of the decay rates. We do not attempt to fit our models to individual runs. The behavior of α_- is no better than those shown in Fig. 5 for α_+. We regard this level of variation as unacceptably large in contrast to the variation in the other two models (cf. Fig. 6a). Model A with constant α_+ leads to large errors in estimates of instantaneous decay rates, and integrating (13) to find the time dependence of Z_+^2 would produce even worse errors. Consequently, we discard Model A as a viable option. While there are many weaknesses in any such simple turbulence model, the main difficulty here seems to be the strong influence of the Alfvén time dependence in Eqs. (17) and (16). This will enter the discussion later in the paper.

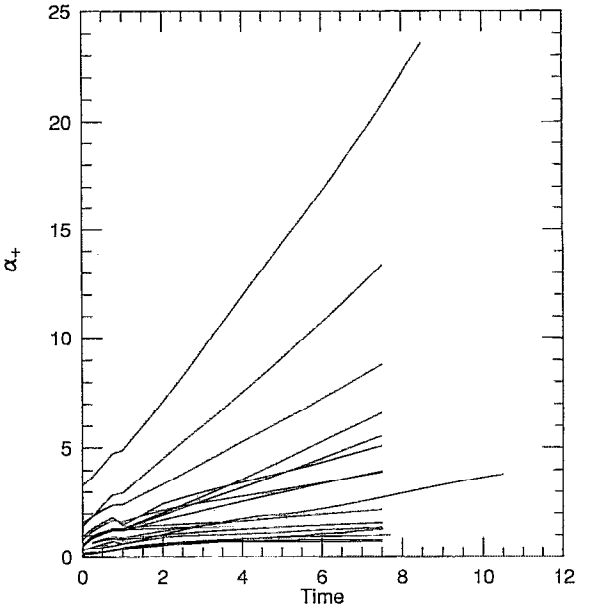

FIG. 5. Computed α_+ from simulation data using Model A for all MHD runs. A good model would show all curves saturated at an order unity constant. Large and non-constant α_+ indicate poor agreement with the model. The α_- display similar disagreement (not shown).

B. Decay rates in Models B1 and B2

When examining decay rates as we did in the previous section, the dynamical equations for the length scales do not enter the procedure, since λ_+, λ_-, and, if needed λ, are directly evaluated from simulation data. Similarly, when separate values of the two length scales are used in Models B1 and B2, there is no distinction between the two models if only the $Z_\pm^2$ decay rates are computed. Following the approach described above, we evaluate the accuracy and time stability of α_+ and α_- by calculating the right hand sides of (31) and (32) from simulation data and comparing these Model B estimates of $dZ_\pm^2/dt$ with finite difference values of the same quantities from the simulation records of $Z_\pm^2(t)$.

First we consider results from simulations having no mean magnetic field, i.e., $B_0=0$ (Table I). For these runs, Fig. 6 illustrates the values of $\alpha_\pm$ computed in the way described above. The time history of α_+ in Fig. 6a reveals the accuracy of Model decay rates for Z_+^2 (called the majority

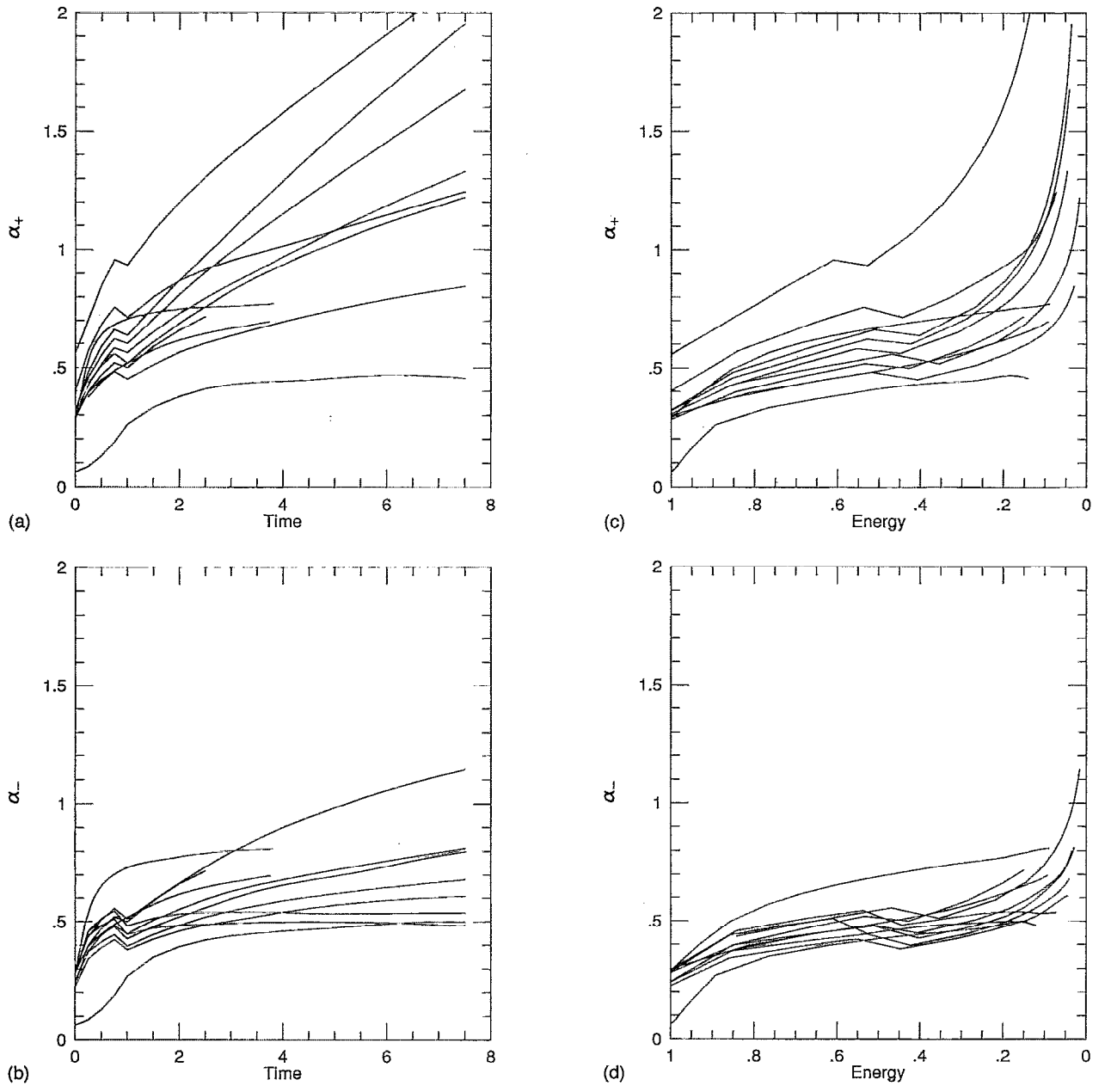

FIG. 6. Computed (a) α_+ and (b) α_- versus time and (c) α_+ and (d) α_- versus energy from simulation data using Model B2 for all MHD runs with no mean magnetic fields. In contrast to Fig. 5 for Model A these figures show much better agreement between the simulation and Model B, In particular, (c) and (d) show a range of energies for which the model produces adequate agreement. Relatively poor fit curves correspond to high cross helicity runs.

species because initial values have $Z_+^2 \geqslant Z_-^2$). For the full range of parameters in these simulations, α_+ varies by no more than about a factor of two, the central value lying between 0.5 and 1 in the later times of Fig. 6a. Unlike the results of Model A (note the scale change in ordinate), all values in Model B are less than about 2.0 for $t<8$. The calculated values of α_- shown in Figure 6b for the same runs are even more tightly clustered, with $0.4<\alpha_-<1.0$ during $2<t<7$ for almost all runs. It is therefore possible to choose values of both $\alpha_\pm$ in the range of about 0.5 to 1.0 and get reasonably good decay rates from the Model B formulae for runs with $B_0=0$. We note a systematic trend in Figs. 6a and 6b that the Model B decay rate systematically falls behind the actual decay rate as time progresses, i.e., larger values of α are indicated at later times. This may in part be caused by the limitations on our simulations for sustaining truly turbulent behavior for many characteristic times. At late times the fields are small and then the nonlinear terms in the dynamical equations are negligible compared to the linear dissipative decay term. The latter implies exponential decay in time. The late time trend in Figs. 6a and 6b may also in part be related to the fact that these phenomenological models possesses conservation properties discussed in sections IV B and C. The conservation property would force a slow down of the Z_+ field if Z_- is small. This built-in conservation property emulates a property of the pointwise full MHD

equations. If one of the Elsässer variables is zero then the spectral transfer ceases completely. But this conservation property may not be an exact property of MHD. In addition, there is a rapid increase in $\alpha_{\pm}$ very early in the runs, suggesting a transient startup period during which the correlations associated with turbulent spectral transfer are being established. To partially account for these effects, we present the same data again in Fig. 6c and Fig. 6d, now plotted against total energy remaining in the turbulence rather than against time. These figures exhibit an extended interval, the energy range of about $0.9>E>0.2$, during which the curves of $\alpha_{\pm}$ are relatively flat or stable.

We turn now to the performance of Model B in runs having non-zero values of B_0. Figure 7 shows values of $\alpha_{\pm}$ determined as described above and plotted vs. energy. Once again we see that Model B estimates decay rates of $Z_{\pm}^2$ in reasonable agreement with those directly computed. The ratios of estimated to computed decay rates again cluster about a central value of order unity, though perhaps at a slightly lower value than for the $B_0=0$ runs. In fact, the clustering is possibly better for runs with non-zero B_0. A general estimate $\alpha_{\pm}\approx 0.4$ seems appropriate for runs with non-zero mean magnetic field.

C. Time evolution in Models B1 and B2

Model B predicts instantaneous decay rates well enough that we will examine its predictions in greater detail. In the previous subsection, the differences between Model B1 and Model B2 were minimal since the evolution equations for the length scales were not used. A stronger challenge for the models is to compare the computed time history from the model with that from the simulations. Also, models B1 and B2 now differ, B2 having two length-scales governed by (30), while B1 has a single length-scale satisfying (23). To eliminate the influence of initial transients, we use data from $t=1$ as the initial parameters in the models, and compare their predictions with the simulations after that time. Some of our parameter fits are designated as optimized, by which we mean a rough trial and error procedure.

In Fig. 8 we illustrate such a comparison for Run 07, which begins with zero cross helicity, unit Alfvén ratio, and $B_0=0$. This run is in some ways quite similar to a Navier–Stokes run (see section VII B). Figure 8a shows the time history of Z_+^2 and Z_-^2 from the simulation between $t=0$ and 4. The integrated model solutions shown on the same panel use $\alpha_+=\alpha_-=0.8$, $\beta_+=0.45$, and $\beta_-=0.60$. For the same simulation, Fig. 8b shows the evolution of the two length scales $\lambda_{\pm}$ defined in Eq. (12) and compared to the model predictions in the same way. The behavior of the model is reasonable but far from exact. However, comparing these results for Run 07, a "pseudo-Navier–Stokes" run, with Figs. 4c and 4d, we see that the Model B2 predictions are of the same level of accuracy as the simple hydrodynamic model in accounting for the energy decay in the hydrodynamic simulation.

In Fig. 9, Model B2 is compared with Run 15, a simulation with relatively high cross helicity, a high Alfvén ratio (kinetic/magnetic energy $=3$), and $B_0=0$. Again the modeled evolution commences at simulation time $t=1$. Note that Fig. 9 displays two model solutions. In one, the model solutions use parameters optimized for that simulation ($\alpha_+=1.3$, $\alpha_-=0.8$, $\beta_+=0.5$, $\beta_-=0.3$). In the other case, typical parameters found from the average behavior of the full set of simulations are used ($\alpha_+=1.0$, $\beta_+=0.5$). We can see that with the optimized constants, the model is again accurate at a reasonable level, but for the non-optimized typical constants, the results are much less satisfactory.

As a third and final example of Model B's ability to predict global energy decay, we examine Run 20, which has a strong mean magnetic field $B_0=8$. Here the initial values

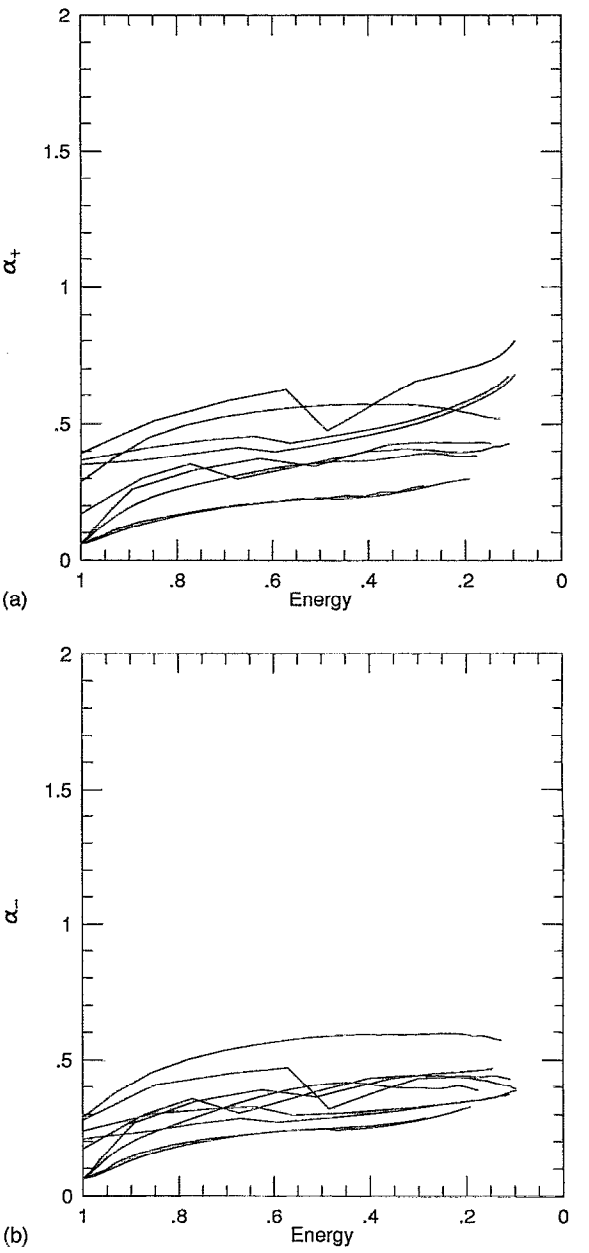

FIG. 7. (a) α_+ and (b) α_- versus energy from simulation data using Model B2 for all MHD runs with non-zero mean magnetic fields. A relatively good agreement (except lower values of α's) indicates weak dependence of decay rates on the mean magnetic fields.

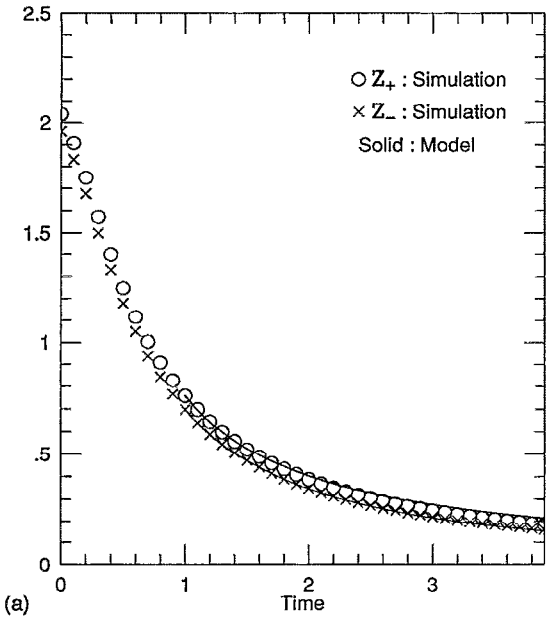

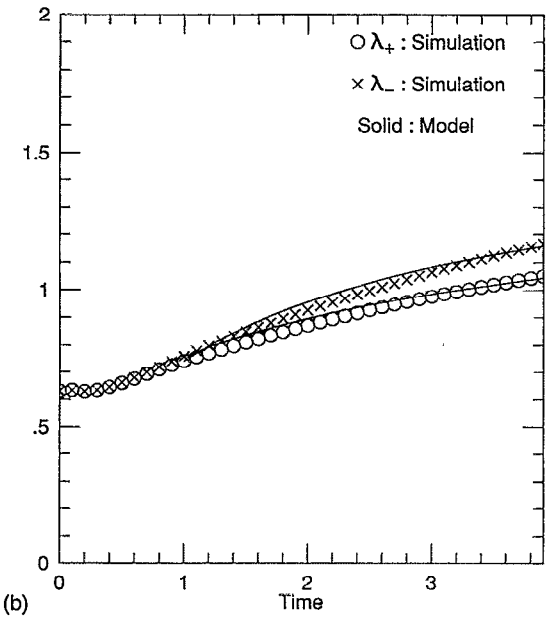

FIG. 8. Evolution of (a) $Z_{\pm}^2$ and (b) $\lambda_{\pm}$ obtained by integrating Model B2 for Run 07 using best fit values of $\alpha_{\pm}$ and $\beta_{\pm}$ starting form $t=1$. The discrete points are from the simulation.

used in the model are taken from $t=4$ because the transients persist much longer. The results are shown in Fig. 10, for both optimized model parameters ($\alpha_{\pm}=0.3$, $\beta_{\pm}=0.4$), and for the typical values of model constants used above in the Run 15 comparison. Once again we see a reasonably good level of prediction of energy decay for the optimized constants but less satisfactory performance for the typical constants.

VI. REFINEMENTS

A. Spectral anisotropy

The above discussion indicates that lower values of the energy decay constants are needed in Model B with finite

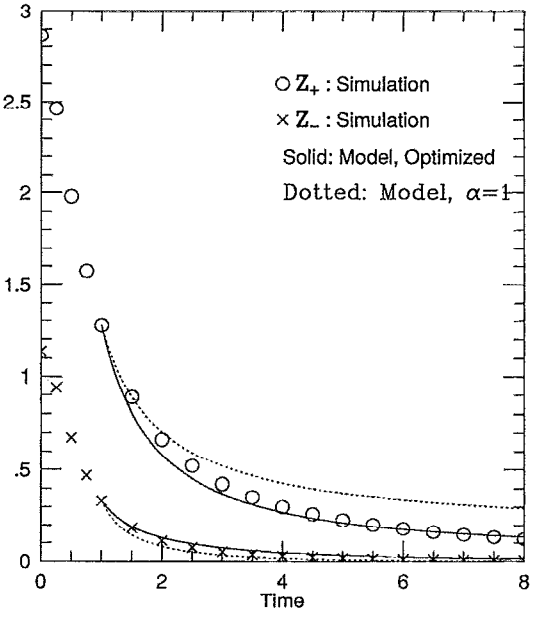

FIG. 9. Evolution of $Z_{\pm}^2$ obtained by integrating Model B2 for Run 15 using the best fit values of $\alpha_{\pm}$ and $\beta_{\pm}$ (solid lines) and using $\alpha_{\pm}=1$ (dotted lines).

B_0 compared to cases when $B_0=0$. This follows because the effective values of α in runs with mean magnetic fields were lower than in the $B_0=0$ runs. The same conclusion was apparent from Fig. 10 when two solutions of Model B with optimized and typical α's were tested against the time history of Run 20, which has a strong mean magnetic field. Model B does not include any effects of Alfvénic decorrelation in the sense of (16) and (17). In contrast, such effects were intended to be present in Model A, through dependence

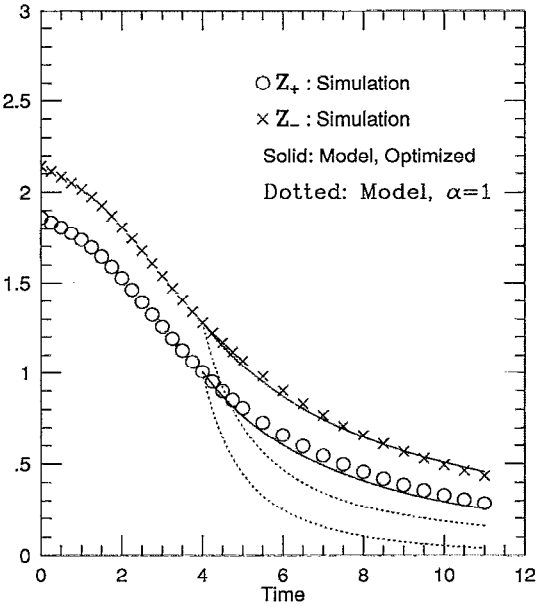

FIG. 10. Evolution of $Z_{\pm}^2$ obtained by integrating Model B2 for Run 20 using the best fit values of $\alpha_{\pm}$ and $\beta_{\pm}$ (solid lines) and using $\alpha_{\pm}=1$ (dotted lines).

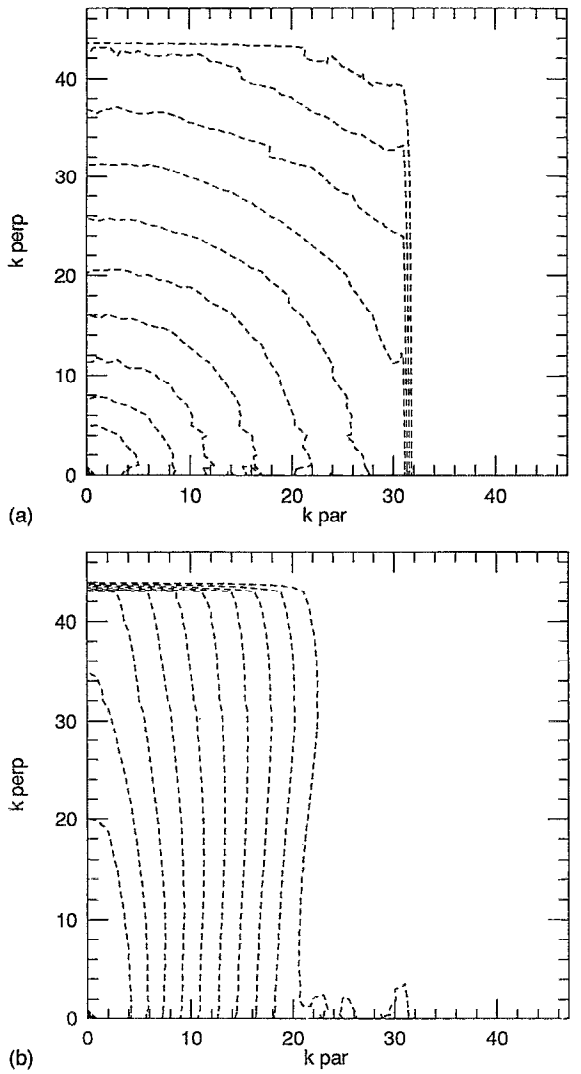

FIG. 11. Contours of modal magnetic energy spectrum at the end of the run for (a) Run 07 and (b) Run 20 in $k_{\|}$-$k_{\perp}$ space. Clearly Run 20 with high external magnetic field shows a high degree of anisotropy. (a) for Run 07 with no mean magnetic field shows relatively isotropic spectrum.

of $\tau_s^{\pm}$ upon τ_A and thus upon both B_0 and the rms fluctuation b. However, the calculated decay "constants" for Model A varied by an unacceptably large amount, especially for runs with a large mean magnetic field and/or large cross helicity.

Both of these observations can be understood by appealing to the effects of spectral anisotropy. Numerical simulations of both freely decaying[37–39] and driven[40] turbulence have shown that wavenumber spectra in dissipative MHD turbulence become distinctly anisotropic in the presence of a uniform mean magnetic field of sufficient strength. This anisotropy is consistent with relatively rapid spectral transfer in wave-vector directions that are nearly perpendicular to the mean field and accordingly slower spectral transfer parallel to the mean field. This phenomenon has been described in terms of a resonance argument.[37]

Spectral anisotropy is clearly seen in the present simulation data base even though the initially loaded fluctuation spectra are all isotropic. Figure 11 shows the energy spectrum at the end of the simulation for two runs as a function of $k_{\perp}=|\mathbf{k}-k_{\|}\hat{\mathbf{z}}|$ and $k_{\|}=\mathbf{k}\cdot\hat{\mathbf{z}}$, where the mean field is $\mathbf{B}_0=B_0\hat{\mathbf{z}}$. Panel 11a shows that the spectrum for Run 07 with $B_0=0$ remains almost completely isotropic. However, the spectrum in Run 20 becomes highly anisotropic as is illustrated in Panel 11b. As the above spectral transfer arguments predict, the contours are extended further in the perpendicular direction, indicating preferential spectral transfer towards smaller scales with variations transverse to the mean field.

The main distinction between Models A and B is in the way that Alfvénic decorrelation effects are handled. In Model A, all wave-vectors experience the full decorrelation effect of the mean field $\mathbf{B}_0$, as though they were all aligned with the mean field. Model B on the other hand represents the opposite extreme: there is no Alfvénic decorrelation effect, as if all wave-vectors were perpendicular to $\mathbf{B}_0$. Run 20 indicates a situation intermediate to these two extremes. The increased anisotropy due to enhanced perpendicular transfer evidently tends to suppress Alfvénic decorrelation effects. In the inertial range this effect modifies the effective Alfvén time from $\tau_A(\mathbf{k})=(kB_0)^{-1}$, a value appropriate for slab turbulence, to $|\mathbf{k}\cdot\mathbf{B}_0|^{-1}$, so that the angle of $\mathbf{k}$ relative to the mean field $\mathbf{B}_0$ enters explicitly. An anisotropic version of τ_s is also appropriate for the energy-containing range, where the spectral transfer rate [cf. (17)] for anisotropic turbulence should be modified to read

$$\frac{1}{\tau_s^{\pm}}=\frac{Z_{\mp}^2}{\lambda_{\pm}}\frac{1}{(Z_{\mp}+B_0\cos\theta_{\pm})}, \tag{41}$$

where $\cos\theta_{\pm}$ measures the degree of anisotropy[37,38] of the $z_{\pm}$ spectrum in the energy-containing range.

We attempt to account for anisotropy by using the spectral transfer rate (41) to modify the decay equations (13), producing a model that is a hybrid of Model A and B. However, no dependence of τ_A upon b is retained (see discussions in the summary section). Figure 12 shows the results of the anisotropy-modified model for Run 20 with $B_0=8$. The values of the anisotropy angles used are $\cos\theta_+=0.3$ and $\cos\theta_-=0.2$, while $\alpha_+=\alpha_-=1$. Again applying the model solutions only after $t=4$, we see that the anisotropic model is reasonably accurate for both $Z_+^2(t)$ and $Z_-^2(t)$ and works about as well as Model B1 with optimized constants $\alpha_{\pm}$.

The anisotropic model for simulations with $B_0\neq 0$ admits a plausible physical interpretation. However, one needs to know how θ scales with B_0 and other factors such as Reynolds number. In principle, θ can also depend upon time or energy. Some similar simulations[38] suggest that anisotropy increases with time, Reynolds number, and/or B_0. One possibility, suggested by the clustering of decay rate ratios in Fig. 7 for several different values of B_0, is that $\theta_{\pm}$ satisfies $Z_{\pm}+B_0\cos\theta_{\pm}\approx 2Z_{\pm}$. This has the effect of halving the decay rate relative to the $B_0=0$ value, roughly consistent with the numerical results. This approximation has the simple interpretation that $\cos\theta=b/B_0$, which also emerges from anisotropic theories of reduced MHD.[41] To illustrate this scaling we plot in Fig. 13 the quantity $B_0\cos\theta_-/Z_+$ synthesized from the decay rates for Z_- in simulation runs with non-zero B_0 in the same spirit used in $\alpha_{\pm}$ computations of sections V A and V B. Here we have used (41) for τ_s^-. Figure 13 shows that

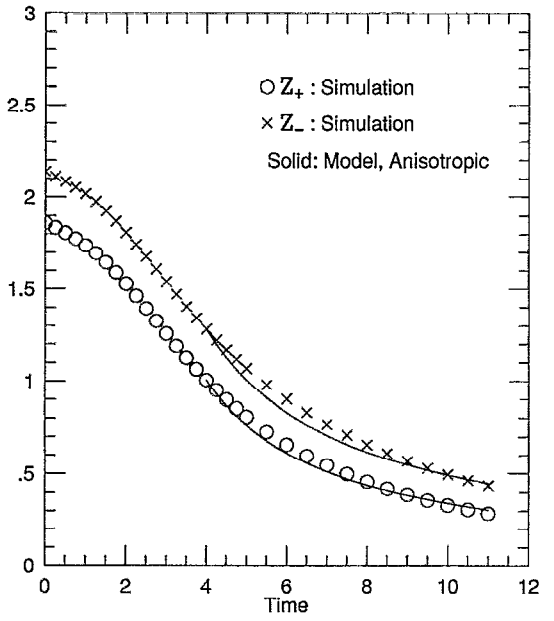

FIG. 12. Evolution of $Z_{\pm}^2$ obtained by integrating Model B2 with an anisotropic correction for Run 20.

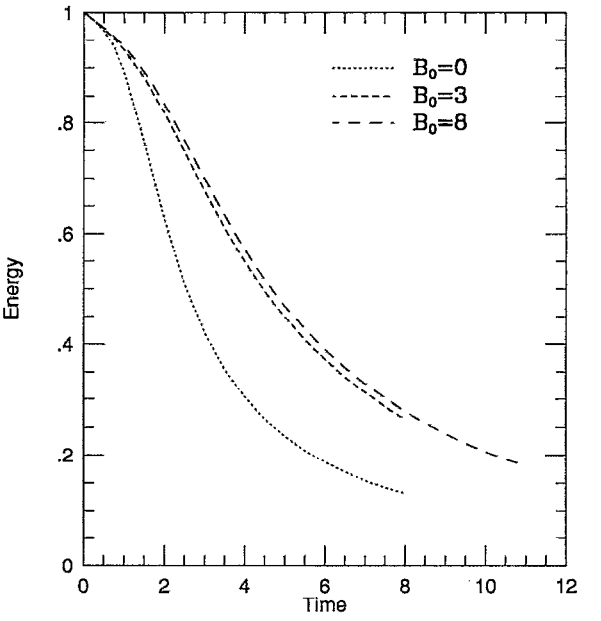

FIG. 14. Time evolution of total energy for three runs with $B_0=0$, 3 and 8. Note the large changes in the decay rates as B_0 increase from 0 to 3, and the lack of change for further increases in B_0.

all curves have the tendencies to saturate in the neighborhood of unity. The spread of the curves surely decreases as a function of time. If all curves approach unity then the above discussion about halving of the decay rates for non-zero B_0 runs relative to the $B_0=0$ runs would exactly hold true. Similar behavior is seen in synthesized $B_0\cos\theta_+/Z_-$ (not shown here).

While further study of the anisotropy effect is warranted, at present we note that one implication of the above hypothesis is that decay rates become independent of B_0 once the mean field is strong enough to produce significant anisotropy. We can see some evidence in support of this by comparing the time histories of three runs that are identical except for their values of B_0. This is illustrated in Fig. 14, for runs having $B_0=0$, 3, and 8. A large difference is seen between cases with zero mean field and $B_0=3$, but very little additional difference is seen when B_0 is raised to 8.

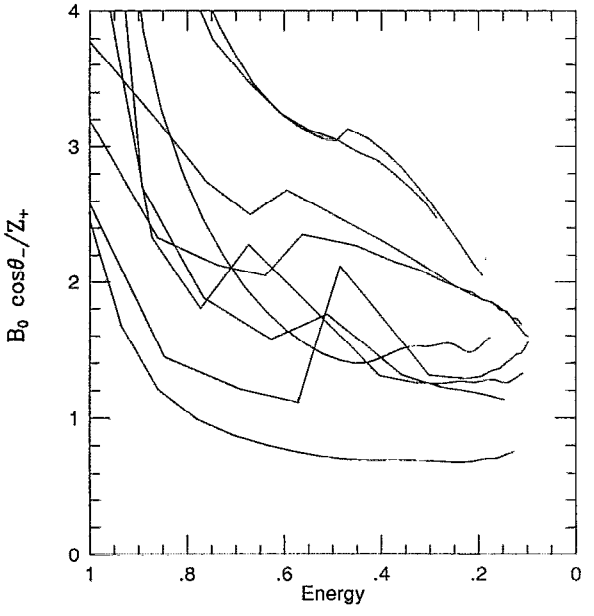

FIG. 13. Computed $B_0\cos\theta_-/Z_+$ from simulation data using Model A for all MHD runs with non-zero B_0.

B. Behavior of the energy difference

The models discussed so far have not dealt explicitly with the energy difference D. The main reason is that we have applied the models after the startup transient period that lasts about a nonlinear time, and during that phase most of the initial D (if any) decays to zero. After that D maintains a small negative value (if $B_0=0$) or is very small. When the mean field is strong enough, D oscillates about zero. In addition, the dynamical equations for the fields $Z_{\pm}$ and $\lambda_{\pm}$ that we adopted in the models do not involve D. However we might inquire as to how accurate a very simple time-dependent model for D might be.

Estimating the turbulent decay rate of D is not as straightforward as for $Z_{\pm}^2$, because it is not conserved by nonlinear interactions in either the energy-containing or the inertial range. However, from closure equations[7] and perturbative arguments[42] (similar to weak turbulence theory), one can argue that D tends to relax toward zero. This conjectured tendency toward equipartition of MHD energy between magnetic and kinetic ingredients is known as the Alfvén effect.[6,7,42] However, equipartition must be adopted with caution. There are a number of indications that magnetic energy in the inertial range may be somewhat larger than the kinetic energy, from closures,[7,11] solar wind observations,[43–45] and MHD simulations.[46–48] At the larger scales that tend to dominate the energy budget, there are additional effects, such as inverse cascades[18,13] and dynamo action that might cause

excess total magnetic energy. Mechanisms for generating turbulence might give rise to excess kinetic energy, e.g., due to large-scale shear flows. These and other factors may complicate the development of a very accurate model for $D(t)$.

Here we adopt a simplified approach, based upon the discussions presented by Pouquet *et al.*,[7,11] and Mangeney *et al.*,[49] and presented previously in Matthaeus *et al.*[36] The model is

$$\frac{dD}{dt} = -\frac{D}{\tau_A} - \frac{u^2}{\tau^*}, \tag{42}$$

where τ^* is defined as the time scale for decay of the total energy, $\tau^* = -(Z_+^2 + Z_-^2)/(\dot{Z}_+^2 + \dot{Z}_-^2)$. Here $\tau_A = \lambda/B_0$ is the Alfvénic time associated with the single length scale λ, defined just below Eq. (12).

We will not dwell upon a justification for this model here, since it is considered as reasonable but somewhat *ad hoc*. We note simply that the right hand side incorporates two effects. First, the dynamical tendency for the energy difference to decay toward zero due to the Alfvén effect is modeled by a relaxation time $\tau_A = \lambda/B_0$, in accord with the suggestion of Pouquet *et al.*[7] Second, the net effect of transfer of D towards finer scales is estimated following the arguments of Grappin *et al.*[11] for the inertial range. The essence of their reasoning is that D is driven at a rate equal to the net direct spectral transfer rate of the energy. We have given a variation of this argument[36] in which just the kinetic energy u^2 appears in the direct transfer term, and we adapt this approach to the energy-containing range, giving rise to the second term in Eq. (42). The sign of the direct transfer term is selected to agree with simulations and observations, in which an excess of magnetic energy is frequently seen. Note that when the total magnetic field vanishes, Eq. (42) reduces to the ordinary ($\alpha = 1$) hydrodynamic decay model, Eq. (3).

We employed Eq. (42) to approximate the time histories of $D(t)$ from the simulation data base. Figure 15 depicts the time histories from Run 07, 15, and 18, all of which have a $B_0 = 0$ (for $B_0 = 0$ runs, $D \to 0$ rapidly with subsequent oscillations). Runs 15 and 18 initially had excess kinetic energy (Table I). In these two simulations, D decays rapidly towards zero, over roughly a nonlinear time, and remains there subsequently. This is also seen in the model results. For Run 18, which has more robust decay due to lower cross helicity, the model overshoots and gives a negative tail much larger than the simulation itself, near about $t = 2$. For the remaining case, Run 07, there is equipartition initially and zero cross helicity. Again there is qualitative agreement for the model, which predicts a negative bias initially, as seen in the simulation. However, it remains negative for too long a time. These results for the time dependent D model are somewhat reasonable, but not extremely accurate. We defer investigation of further developments regarding $D(t)$, recalling that the energy decay models work best after the transient period, and that D has approached zero to a reasonable approximation by that time, in both the model and the simulations.

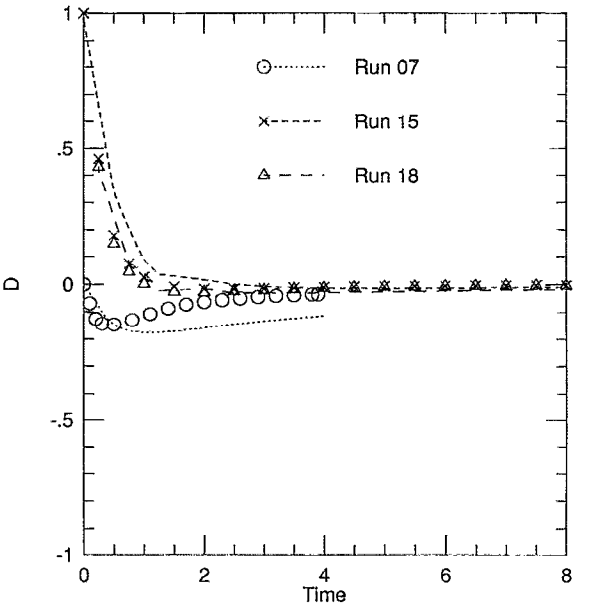

FIG. 15. Time evolution of D from the model (dotted and dashed lines as in legend) and from the simulations (symbols).

VII. FURTHER ANALYSIS OF THE MODELS

A. Dynamic alignment

It is widely recognized[21,50,8] that the MHD equations exhibit tendencies of dynamic alignment, by which we mean that the magnitude of the normalized cross helicity σ_c grows in time. Dynamic alignment is not proven to be a universal property of all MHD solutions, and indeed, there are situations, such as the radially evolving solar wind,[45] or homogeneous turbulence with strong shears[51] in which alignment is known not to occur. However, it is generally thought that homogeneous MHD turbulence lacking a strong magnetic inverse cascade and lacking strong velocity shears, will usually engage in dynamic alignment. Even these two exceptional cases might well display dynamic alignment after an initial transient period. In many cases[52,17] a certain amount of dynamic alignment, even if non-monotonic, accompanies other MHD relaxation processes.

The question is, do the models for the decay of energy-containing eddies presented in section IV also show the tendencies of dynamic alignment in the mean? Here we take this to mean: does the normalized cross helicity $\sigma_c = 2H_c/E$ show monotonic growth towards $\sigma_c = \pm 1$? (The sign is determined by the initial conditions.)

Let us examine the time rate of change of σ_c,

$$\frac{d\sigma_c}{dt} = \frac{d}{dt}\left[\frac{Z_+^2 - Z_-^2}{Z_+^2 + Z_-^2}\right]. \tag{43}$$

For simplicity, we use the two later models (B1 and B2) in evaluating the right hand side of (43). We assume that the majority (minority) species is the larger (smaller) Elsässer field and that $Z_+^2 > Z_-^2$. A straightforward substitution gives:

$$\frac{d\sigma_c}{dt} = \frac{2Z_+^2 Z_-^2}{E^2}\left[\frac{\alpha_-}{\lambda_-} Z_+ - \frac{\alpha_+}{\lambda_+} Z_-\right]. \tag{44}$$

Here, E is the sum of the two fields $Z_+^2+Z_-^2$. Therefore, for $\alpha_+\lambda_-Z_-<\alpha_-\lambda_+Z_+$ the sign of $d\sigma/dt$ is preserved. Implicit in this is that the $Z_\pm$ versus time curves never cross each other. If on the other hand $\alpha_+\lambda_-Z_->\alpha_-\lambda_+Z_+$, σ_c can evolve in the opposite direction to dynamic alignment. Often for simplicity we want to use symmetrical models having $\alpha_+=\alpha_-$. In those cases, the above condition implies dynamic alignment whenever the length scales λ_+ and λ_- are not too dissimilar. By constructing a situation in which the minority species resides at very much longer wavelength than the majority species, departures from dynamic alignment can be achieved. Clearly in a symmetric single length scale model, dynamic alignment always occurs.

B. Navier–Stokes limit of MHD

There are two separate limits which are related to Navier–Stokes turbulence. First, if Z_+ and Z_- are equal, then both Model B1 and Model B2 have the same structure as the model for Navier–Stokes turbulence, Eqs. (3) and (4). In this limit $\mathbf{b}\neq\mathbf{0}$, but the velocity and magnetic fields have analogous roles. Second, in terms of the primitive variable equations, reduction to Navier–Stokes flow requires that $\mathbf{z}_+=\mathbf{z}_-$ pointwise (i.e., $\mathbf{b}\to\mathbf{0}$). This state, with high electrical conductivity may be susceptible to instabilities that give rise to dynamo action, the permanent generation of an energetically significant magnetic field. In the models, the pointwise reduction to hydrodynamics implies that the normalized energy difference $\sigma_D=(u^2-b^2)/(u^2+b^2)$ take on its maximal value of 1. However, dynamo instability can lead to $\sigma_D\leqslant 0$ later.

In these models we have not considered including the evolution of D in the dynamical equations for the energies $Z_\pm^2$. Therefore, we cannot address the issue of whether maximal D or vanishing D brings the decay rates of MHD most closely into accord with Navier–Stokes turbulence. However the simulations [along with the simple model for $D(t)$] shows that D vanishes very quickly during the transient phase. This may suggest that the only requirement for the hydrodynamic analogy within the context of the decay models is the equality of Z_+ and Z_-, i.e., zero cross helicity. In connection with this, it is notable that the typical values of $\alpha_+=\alpha_-=0.8$ and $\beta_+=\beta_-=0.5$ compare quite reasonably to typical values for the hydrodynamic model of $\alpha=0.9$ and $\beta=0.5$. Thus, a run like Run 07 which has $Z_+=Z_-$ can be thought of as a pseudo Navier–Stokes run.

C. Is vanishing cross helicity a maximal decay state?

All three models for MHD energy decay described above yield stationary states when one of the fields $Z_\pm$ is zero. This property is built-in to emulate the property of the full set of MHD equations, that time evolution ceases if one of the Elsässer variables $\mathbf{z}_\pm(\mathbf{x},t)$ vanishes. Thus we have no spectral transfer with maximal cross helicity, $\sigma_c=\pm 1$. To what extent is increasing cross helicity associated with decreasing energy decay rate? Dynamic alignment provides at least heuristic support for the assertion that cross helicity decreases decay rates, since it is associated with an ideal conservation law. To the extent that this constraint is more restrictive when $|\sigma_c|$ is large, one would expect smaller maximum possible decay rates of energy. In spite of intuition regarding this issue, like the dynamic alignment process itself, the question of whether vanishing cross helicity is a maximal energy decay state remains unanswered for the MHD equations, as far as we are aware. How about the same issue in the models for decay?

Let us take a simple model where λ is constant and we consider only the evolution of Z_+^2 and Z_-^2

$$\frac{dZ_+^2}{dt}=-\alpha Z_+^2 Z_-, \tag{45}$$

$$\frac{dZ_-^2}{dt}=-Z_-^2 Z_+. \tag{46}$$

We can use only one α without loss of generality. The statement that $\alpha=1$ in this special case corresponds to the symmetric model with $\alpha_+=\alpha_-$ in the notation of the rest of the paper. Let us define the energy E to be $Z_+^2+Z_-^2$. We re-write the evolution of total energy E in terms of one of the fields, say, $Z_-^2=y$:

$$\gamma=-\frac{dE}{dt}=\alpha(E-y)\sqrt{y}+y\sqrt{E-y}. \tag{47}$$

By inspection we see that the well known result that if cross helicity is maximal, i.e., y is zero or equal to E, then the decay rate vanishes. To find the maximum decay rate we differentiate (47) with respect to y:

$$\frac{d\gamma}{dy}=\frac{1}{\sqrt{y}\sqrt{E-y}}\left[\frac{\alpha}{2}(E-y)^{3/2}-\alpha y(E-y)^{1/2}-\frac{1}{2}y^{3/2}+y^{1/2}(E-y)\right]. \tag{48}$$

For $\alpha=1$, the curve (47) has a maximum at $y=E/2$ [i.e., the r.h.s. of (48) is zero] and is symmetric about this point. That is, for zero cross helicity, the energy decay rate is maximum. For the general case when $\alpha\neq 1$, then the curve is not symmetric about $y=E/2$ and the maximum decay rate does not occur at $y=E/2$. Thus, there exists a non-zero cross helicity for which the decay rate of energy is maximal. The conclusion is that one must use symmetric models with $\alpha_+=\alpha_-$ to maintain the intuitive (but in general unproven) property that zero cross helicity should correspond to a state of maximal energy decay.

D. Cross helicity and conservation laws

Dynamic alignment appears to be associated with the constraint of inviscid conservation of cross helicity.[21,17] This conservation property is a constraint on the nonlinear couplings in the incompressible MHD equations. When small but finite viscous or Ohmic dissipation coefficients are present, the conservation law is broken, and one would expect in general that some cross helicity decay will accompany decay of the Elsässer energies. Approximate conservation of cross helicity has formed the basis for a number of

theoretical treatments of dynamic alignment and other MHD relaxation processes,[52,17] and it is an exact property of the phenomenology.[21]

Unfortunately, there is no indication in the present study (or in others as far as we are aware) that there is an exact conservation law related to the cross helicity at large but finite Reynolds numbers. In all cases there is indication of cross helicity decay (temporal changes in $Z_+^2 - Z_-^2$), as well as decay of related quantities such as $Z_+ - Z_-$. However, we have not been able to examine all possibilities, such as $Z_+^p - CZ_-^p$ for arbitrary p and C. It is noteworthy that each of the phenomenological models examined in the present study possesses conservation laws of these types. For example, see Eqs. (24) and (33). These conservation laws each produce distinctive behavior of the model solutions both at long times and at large values of cross helicity. (When dynamic alignment is active, these two cases are connected.) Consequently, especially in large σ_c runs, the decay phenomenologies become less accurate. This is usually indicated by a late time change in the effective values of $\alpha_\pm$ as we saw in Figs. 6 and 7. This problem appears to be intimately associated with the fact that the conservation laws in the model do not accurately reflect conservation properties of the exact MHD equations.

VIII. SUMMARY

In this paper we have investigated several phenomenological models for incompressible MHD turbulence. Energy decay in these simple one-point models involves only the two Elsässer energies and their associated length-scales. The large-scale Alfvén speed enters as a parameter, as does possibly a measure of the spectral anisotropy. We also discussed a model for the energy difference that did not influence the energy decay itself. Based upon comparisons of simulation results and predictions of the models, we came to several main conclusions which we summarize here.

The straightforward extension of Kraichnan's[6] inertial range phenomenology to the energy-containing range does not work as well as a simple energy decay model of the Karman-Kolmogoroff type, in which there is no explicit dependence of the modeled spectral transfer and decay rates upon either the large-scale Alfvén speed or that associated with the rms value of **b**. There is some influence of the Alfvén speed upon the simulation results however.

A better performing and more physically appealing model is produced by taking spectral anisotropy into account. This produces a model that is conceptually related to both those discussed above [Models A and B]. This model has the energy decay equations:

$$\frac{dZ_\pm^2}{dt} = -\frac{1}{A}\frac{Z_\pm^2 Z_\mp}{\lambda_\pm} \tag{49}$$

where the parameter $A \approx 1$ when $B_0 \approx 0$, and $A \approx 2$ when $B_0 \geq 1$. This parameter emulates the effects of spectral anisotropy.[37–39] Along with Eq. (49), we have suggested use of an equation for the correlation length scales $\lambda_\pm$. The length scale equations have not been very well-tested in the present study, largely because finite box size constrains the evolution. With present computer capabilities, it appears to be very difficult to examine the unconstrained length scale evolution. Nevertheless the length scale models appear to behave qualitatively correctly relative to the simulation results. In terms of physical motivation, we have somewhat of a preference, given its simplicity, for the length scale equations in Model B2, namely,

$$\frac{d\lambda_\pm}{dt} = \beta_\pm Z_\mp . \tag{50}$$

Finally, we adapted a model equation for the energy difference D from earlier theoretical suggestions.[7,11,36,49] The equation we examined is

$$\frac{dD}{dt} = -\frac{D}{\tau_A} - \frac{u^2}{\tau^*} , \tag{51}$$

where τ^* is defined as the time scale for decay of the total energy, and $\tau_A = \lambda / V_A$ is the Alfvén period of the energy-containing eddies. In many cases we found it convenient to deal with the single composite correlation scale $\lambda = (Z_+^2 \lambda_+ + Z_-^2 \lambda_-)/(Z_+^2 + Z_-^2)$.

We have found that the performance of all of the models examined, including the above best-effort model, becomes less acceptable at very large cross helicities and at late times. We have argued that this is due to the fact that all of these models have some conservation law associated with or related to the cross helicity. Such a conservation law is responsible for the ability of the model to display dynamic alignment in time, as is observed in the simulations. However, the models' conservation laws are not exact properties of MHD, and cause errors in the limits in which they play the strongest role. This stands as a challenge to future theory: to find a simple but improved conservation law which permits improved model performance at high cross helicity.

The energy difference model, like the length-scale dynamical models, did not perform as accurately in the tests as did the decay rates of the energies. In this case, we identified a specific weakness. It appears that the direct transfer term in Eq. (51) is too strong, and is in need of further modifications.

Several additional aspects of the phenomenological models were discussed in section VII, focusing on limiting behavior at small and large cross helicity, and the relationship of MHD models to hydrodynamic ones.

It is completely clear that the level of analytical modeling of MHD turbulence represented by the phenomenological models discussed here will in no way replace detailed examination of MHD theory itself. However, our main conclusion is that relatively simple models of MHD global decay appear to work reasonably well in predicting energy and cross helicity decay rates, for a reasonable range of parameters. The modest criterion used in this assessment is simply that the instantaneous decay rates are estimated correctly within a factor of two or so, for several large-scale nonlinear timescales. We expect that the models examined here will be useful as simple estimates of decay and heating due to MHD turbulence in a number of applications where, at least initially, high accuracy is not crucial.

ACKNOWLEDGMENTS

This research has been supported in part by NASA through the Space Physics Theory Program, Grant No. NAG5-1573, and through the Astrophysics Theory Program, Grant No. NAGW-2456, and by NSF Grant No. ATM 93-18728. Computations were performed at the San Diego Supercomputer Center.

APPENDIX A: INITIAL CONDITIONS

The initial modal spectrum for the velocity has the following form:

$$|\mathbf{u}(\mathbf{k})|^2=\frac{A_v}{1+(k/k_0)^{q_v}}. \tag{A1}$$

This spectrum is almost flat below $k=k_0$ (designated as "knee" in Table I) and has a power law form $\sim k^{-q}$ for wavenumbers larger than k_0. Typically we have used $q_v=11/3$ corresponding to $E(k)\sim k^{-5/3}$. The amplitude of the Fourier modes are set to zero outside of a wavenumber range $k<k_L$ and $k>k_H$. For the excited range, the real part of the Fourier amplitude is determined in terms of potential functions by $Re[\mathbf{u}(\mathbf{k})]\sim(\mathbf{k}\times\hat{\mathbf{z}}g_1-\mathbf{k}\times(\mathbf{k}\times\hat{\mathbf{z}})g_2)|\mathbf{u}(\mathbf{k})|$, where g_1 and g_2 are unit variance Gaussian random numbers. The imaginary part is selected in an equivalent manner. Specific values of k_L and k_H for various runs are listed in Table I as "k-range."

The magnetic modal energy also has a similar form,

$$|\mathbf{b}(\mathbf{k})|^2=\frac{A_b}{1+(k/k_0)^{q_b}}. \tag{A2}$$

Again the spectral shape and a set of random Gaussian numbers are used to select appropriate potentials that enforce the solenoidal property.

The normalizing constants are adjusted after the fact to control the total energy. At this stage the constants A_v to A_b can be adjusted to yield a particular Alfvén ratio r_A. For uncorrelated $\mathbf{v}(\mathbf{k})$ and $\mathbf{b}(\mathbf{k})$ the cross helicity is vanishingly small. To generate a non-vanishing cross helicity, a correlation is introduced between the random numbers selected for the velocity field and those selected for the magnetic field.

APPENDIX B: GENERAL SOLUTION OF MODEL B1

Dividing (26) by (27) we get:

$$\frac{dZ}{d\lambda}=-\frac{\sqrt{Z^2-a^2}}{\lambda}\frac{\tilde{\alpha}}{2\beta}. \tag{B1}$$

This can be integrated to yield:

$$\lambda=\frac{C}{[Z+\sqrt{Z^2-a^2}]^{\gamma}}, \tag{B2}$$

where

$$C=\lambda_0[Z_0+\sqrt{Z_0^2-a^2}]^{\gamma}, \tag{B3}$$

and

$$\gamma=\frac{2\beta}{\tilde{\alpha}}. \tag{B4}$$

Thus, we obtain one equation in Z as a function of time:

$$\frac{dZ}{dt}=\frac{(Z^2-a^2)[Z+\sqrt{Z^2-a^2}]^{\gamma}}{2C}. \tag{B5}$$

Let

$$q=Z+\sqrt{Z^2-a^2}. \tag{B6}$$

In terms of q, (B5) becomes

$$\frac{dq}{dt}=-\frac{1}{4C}(q^2-a^2)q^{\gamma}. \tag{B7}$$

Closed form solutions can be found for integer values of γ. For $\gamma=1$, (B7) has the solution, written in terms of the variable Z,

$$\ln\left[\frac{\sqrt{Z^2-a^2}}{\sqrt{Z_0^2-a^2}}\frac{Z_0+\sqrt{Z_0^2-a^2}}{Z+\sqrt{Z^2-a^2}}\right]=-\frac{a^2}{2C}(t-t_0), \tag{B8}$$

or more revealingly:

$$\frac{a^2}{Z^2}=1-[Ae^{a^2(t-t_0)/2C}-1]^{-2}, \tag{B9}$$

where

$$A=1+\frac{1}{\sqrt{1-a^2/Z_0^2}}. \tag{B10}$$

At long times the right hand side of (B9) approaches unity, and thus Z approaches a. For small values of a we can expand (B9) and (B10). For small a

$$A\approx 2+\frac{a^2}{2Z_0^2}. \tag{B11}$$

By keeping terms of up to order a^2 on the r.h.s. of (B9) we can obtain

$$Z^2=\frac{Z_0^2}{1+\dfrac{Z_0}{\lambda_0}(t-t_0)} \tag{B12}$$

in agreement with (28) for $\gamma=2\beta/\tilde{\alpha}=1$.

[1] P. Bradshaw, T. Cebeci, and J. H. Whitelaw, *Engineering Calculation Methods for Turbulent Flow* (Academic, San Diego, CA, 1981).
[2] J. V. Hollweg and W. Johnson, "Transition region, corona, and solar wind in coronal holes: Some two-fluid models," J. Geophys. Res. **93**, 9547 (1988).
[3] A. Yoshizawa, "Self-consistent turbulent dynamo modeling of reversed field pinches and planetary magnetic fields," Phys. Fluids B **2**, 1589 (1990).
[4] Y. Zhou and W. H. Matthaeus, "Transport and turbulence modeling of solar wind fluctuations," J. Geophys. Res. **95**, 10291 (1990).
[5] E. Marsch and C. Tu, "Dynamics of correlation functions with Elsässer variables for inhomogeneous MHD turbulence," J. Plasma Phys. **41**, 479 (1989).
[6] R. H. Kraichnan, "Inertial-range spectrum of hydromagnetic turbulence," Phys. Fluids **8**, 1385 (1965).
[7] A. Pouquet, U. Frisch, and J. Leorat, "Strong MHD helical turbulence and the nonlinear dynamo effect," J. Fluid Mech. **77**, 321 (1976).
[8] A. Pouquet, M. Meneguzzi, and U. Frisch, "Growth of correlations in magnetohydrodynamic turbulence," Phys. Rev. A **33**, 4266 (1986).
[9] A. Pouquet, M. Meneguzzi, and P. L. Sulem, "Influence of velocity-magnetic field correlations of decaying magnetohydrodynamic turbulence with neutral x points," Phys. Fluids **31**, 2635 (1988).

[10]R. Grappin, U. Frisch, J. Leorat, and A. Pouquet, "Alfvénic fluctuations as asymptotic states of MHD turbulence," Astron. Astrophys. **102**, 6 (1982).
[11]R. Grappin, A. Pouquet, and J. Leorat, "Dependence of MHD turbulence spectra on the velocity field-magnetic field correlation," Astron. Astrophys. **126**, 51 (1983).
[12]W. H. Matthaeus and Y. Zhou, "Extended inertial range phenomenology of magnetohydrodynamic turbulence," Phys. Fluids B **1**, 1929 (1989).
[13]D. Fyfe and D. Montgomery, "High beta turbulence in two-dimensional magnetohydrodynamics," J. Plasma Phys. **16**, 181 (1976).
[14]W. M. Elsässer, "The hydromagnetic equations," Phys. Rev. **79**, 183 (1950).
[15]R. H. Kraichnan, "Helical turbulence and absolute equilibrium," J. Fluid Mech. **59**, 745 (1973).
[16]T. Stribling and W. H. Matthaeus, "Statistical properties of ideal three-dimensional magnetohydrodynamics," Phys. Fluids B **2**, 1979 (1990).
[17]T. Stribling and W. Matthaeus, "Relaxation processes in a low order three dimensional magnetohydrodynamics model," Phys. Fluids B **3**, 1848 (1991).
[18]U. Frisch, A. Pouquet, J. Leorat, and A. Mazure, "Possibility of an inverse cascade of magnetic helicity in magnetohydrodynamic turbulence," J. Fluid Mech. **68**, 769 (1975).
[19]D. Gottlieb and S. A. Orszag, *Numerical Analysis of Spectral Methods: Theory and Applications* (Society for Industrial and Applied Mathematics, Philadelphia, PA, 1977).
[20]C. Canuto, M. Y. Hussaini, A. Quarteroni, and T. A. Zang, *Spectral Methods in Fluid Mechanics* (Springer-Verlag, New York, 1988).
[21]M. Dobrowolny, A. Mangeney, and P. Veltri, "Properties of magnetohydrodynamic turbulence in the solar wind," Astron. Astrophys. **83**, 26 (1980).
[22]M. Dobrowolny, A. Mangeney, and P. Veltri, "Fully developed anisotropic hydromagnetic turbulence in interplanetary space," Phys. Rev. Lett. **45**, 144 (1980).
[23]W. H. Matthaeus, M. L. Goldstein, and D. A. Roberts, "Evidence for the presence of quasi-two-dimensional nearly incompressible fluctuations in the solar wind," J. Geophys. Res. **95**, 20673 (1990).
[24]G. I. Taylor, "Statistical theory of turbulence," Proc. R. Soc. London Ser. A **151**, 421 (1935).
[25]T. de Karman and L. Howarth, "On the statistical theory of isotropic turbulence," Proc. R. Soc. London Ser. A **164**, 192 (1938).
[26]G. K. Batchelor, *Theory of Homogeneous Turbulence* (Cambridge University Press, New York, 1953).
[27]G. K. Batchelor and A. A. Townsend, "Decay of isotropic turbulence in the initial period," Proc. R. Soc. London Ser. A **193**, 327 (1948).
[28]R. W. Stewart and A. A. Townsend, "Similarity and self-preservation in isotropic turbulence," Philos. Trans. R. Soc. London **243**, 48 (1951).
[29]A. N. Kolmogoroff, "Local structure of turbulence in an incompressible fluid for very large Reynolds numbers," Dokl. Akad. Nauk SSSR **30**, 299 (1941a).
[30]A. N. Kolmogoroff, "On degeneration of isotropic turbulence in an incompressible viscous liquid," Dokl. Akad. Nauk SSSR **31**, 538 (1941b).
[31]A. N. Kolmogoroff, "Dissipation of energy in the locally isotropic turbulence," Dokl. Akad. Nauk SSSR **31**, 19 (1941c). This reference, and others relevant to Kolmogoroff theory are reprinted in *Turbulence and Stochastic Processes: Kolmogorov's Ideas 50 Years On*, edited by J. C. R. Hunt, O. M. Phillips, and D. Williams (Royal Society of London, London, 1991).
[32]G. Comte-Bellot and S. Corrsin, "The use of a contraction to improve isotropy of grid-generated turbulence," J. Fluid Mech. **25**, 657 (1966).
[33]P. G. Saffman, "Note on decay of homogeneous turbulence," Phys. Fluids **10**, 1349 (1967).
[34]B. Spalding, "Kolmogorov's two-equation model of turbulence," Proc. R. Soc. London Ser. A **434**, 211 (1991).
[35]M. R. Smith, R. J. Donnelly, N. Goldenfeld, and W. F. Vinen, "Decay of vorticity in homogeneous turbulence," Phys. Rev. Lett. **71**, 2583 (1993).
[36]W. H. Matthaeus, S. Oughton, D. H. Pontius, Jr., and Y. Zhou, "Evolution of energy-containing turbulent eddies in the solar wind," J. Geophys. Res. **99**, 19 (1994).
[37]J. V. Shebalin, W. H. Matthaeus, and D. Montgomery, "Anisotropy in MHD turbulence due to a mean magnetic field," J. Plasma Phys. **29**, 525 (1983).
[38]S. Oughton, E. Priest, and W. Matthaeus, "The influence of a mean magnetic field on 3D MHD turbulence," J. Fluid Mech. **280**, 95 (1994).
[39]V. Carbone and P. Veltri, "A shell model for anisotropic magnetohydrodynamic turbulence," Geophys. Astrophys. Fluid Dyn. **52**, 153 (1990).
[40]M. Hossain, G. Vahala, and D. Montgomery, "Forced magnetohydrodynamic turbulence in a uniform external magnetic field," Phys. Fluids **28**, 3074 (1985).
[41]D. Montgomery, "Major disruptions, inverse cascades and the strauss equations," Phys. Scr. **T2/1**, 83 (1982).
[42]D. Fyfe, D. Montgomery, and G. Joyce, "Dissipative, forced turbulence in two-dimensional magnetohydrodynamics," J. Plasma Phys. **17**, 369 (1977).
[43]W. H. Matthaeus and M. L. Goldstein, "Measurement of the rugged invariants of magnetohydrodynamic turbulence in the solar wind," J. Geophys. Res. **87**, 6011 (1982a).
[44]A. Roberts, M. Goldstein, L. Klein, and W. H. Matthaeus, "The nature and evolution of magnetohydrodynamic fluctuations in the solar wind: Voyager observation," J. Geophys. Res. **92**, 11021 (1987a).
[45]D. A. Roberts, M. Goldstein, L. Klein, and W. H. Matthaeus, "Origin and evolution of fluctuations in the solar wind: Helios observations and Helios-Voyager comparisons," J. Geophys. Res. **92**, 12023 (1987b).
[46]M. Hossain, W. Matthaeus, and D. Montgomery, "Long time states of inverse cascades in the presence of a maximum length scale," J. Plasma Phys. **30**, 479 (1983).
[47]W. H. Matthaeus and S. Lamkin, "Turbulent magnetic reconnection," Phys. Fluids **29**, 2513 (1986).
[48]D. Biskamp and H. Welter, "Dynamics of decaying two-dimensional magnetohydrodynamic turbulence," Phys. Fluids B **1**, 1964 (1989).
[49]A. Mangeney, R. Grappin, and M. Velli, "MHD turbulence in the solar wind," in *Advances in Solar System Magnetohydrodynamics*, edited by E. R. Priest and A. W. Hood (Cambridge University Press, New York, 1991), p. 327.
[50]W. H. Matthaeus and D. Montgomery, "Dynamic alignment and selective decay in MHD," in *Statistical Physics and Chaos in Fusion Plasmas*, edited by C. W. J. Horton and L. E. Reichl (Wiley, New York, 1977), p. 285.
[51]D. Roberts, S. Ghosh, M. Goldstein, and W. H. Matthaeus, "Magnetohydrodynamic simulation of the radial evolution and stream structure of solar wind turbulence," Phys. Rev. Lett. **67**, 3741 (1991).
[52]A. C. Ting, W. H. Matthaeus, and D. Montgomery, "Turbulent relaxation processes in magnetohydrodynamics," Phys. Fluids **29**, 3261 (1986).